

Drivers of nitrogen and phosphorus dynamics in a groundwater-fed urban catchment revealed by high frequency monitoring

Liang Yu^{1,2}, Joachim C. Rozemeijer³, Hans Peter Broers⁴, Boris M. van Breukelen⁵, Jack J. Middelburg⁶, Maarten Ouboter², and Ype van der Velde¹

¹Faculty of Science, Vrije University Amsterdam, 1181HV, Amsterdam, the Netherlands

²Waternet Water Authority, 1096 AC, Amsterdam, the Netherlands

³Deltares, 3508 TC, Utrecht, the Netherlands

⁴TNO Geological Survey of the Netherlands, 3584 CB, Utrecht, the Netherlands

⁵Department of Water Management, Faculty of Civil Engineering and Geosciences, Delft University of Technology, Stevinweg 1, 2628 CN, Delft, the Netherlands

⁶Department of Earth Sciences, Faculty of Geosciences, Utrecht University, P.O. Box 80 021, 3508 TA, Utrecht, the Netherlands

Correspondence to: Liang Yu (xiaobaidrawing@gmail.com)

Abstract. Eutrophication of water bodies has been a problem causing severe degradation of water quality in cities. To gain mechanistic understanding of the temporal dynamics of nitrogen (N) and phosphorus (P) in a groundwater fed low-lying urban polder, we applied high frequency monitoring in Geuzenveld, a polder in the city of Amsterdam. The high frequency monitoring equipment was installed at the pumping station where water leaves the polder. From March 2016 to June 2017, total phosphorus (TP), ammonium (NH₄), turbidity, electrical conductivity (EC), and water temperature were measured at intervals smaller than 20 minutes. This paper discussed the results at three time scales: annual scale, rain event scale, and single pumping event scale. Mixing of upwelling groundwater (main source of N and P) and runoff from precipitation on pavements and roofs was the dominant hydrological process governing the temporal pattern of the EC, while N and P fluxes from the polder were also regulated by primary production and iron transformations. In our groundwater-seepage controlled catchment, NH₄ appeared to be the dominant form of N with surface water concentrations in the range of 2-6 mg N/L, which stems from production in an organic-rich subsurface. The concentrations of NH₄ in the surface water were governed by the mixing process in autumn and winter and were reduced down to 0.1 mg N/L during the algae growing season in spring. The depletion of dissolved NH₄ in spring suggests uptake by primary producers, consistent with high concentrations of chlorophyll-a, O₂, and suspended solids during this period. Total P and turbidity were high during winter (range 0.5-2.5 mg P/L and 200-1800 FNU, respectively) due to the release of P and reduced iron from anoxic sediment to the water column, where Fe²⁺ was rapidly oxidised and precipitated as iron oxides which contributed to turbidity. In the other seasons, P is retained in the sediment by sorption to precipitated iron oxides. Nitrogen is exported from the polder to the receiving waters throughout the whole year, mostly in the form of NH₄, but in the form of organic N in spring. P leaves the polder mainly during winter, primarily associated with Fe(OH)₃ colloids and as dissolved P. Based on this new understanding of the dynamics of N and P in this low lying urban catchment we suggested management strategies that may effectively control and reduce eutrophication in urban polders and receiving downstream waters.

Keywords: Nitrogen and phosphorus dynamic, high frequency monitoring, benthic algae, iron chemistry, Amsterdam, groundwater seepage

1 Introduction

Eutrophication is one of the most notorious phenomena of water quality impairment in cities, caused by excess inputs of N and P. The identified sources of nutrients are from wastewater treatment plants, storm runoff, overflow of sewage systems, manure and fertilizer application in urban green areas and atmospheric deposition (Walsh et al., 2005; Kabenge et al., 2016; Toor et al., 2017; Yang & Toor, 2018; Putt et al., 2019). Recently, groundwater has been identified as another important source

42 of N and P in cities situated in low-lying deltas, where dissolved NH_4 and PO_4 in groundwater seep up into urban surface water
43 (Yu et al., 2018 & 2019). The upwelling nutrients in groundwater, originating from the organic rich delta subsurface, reaching
44 the surface water of cities and are transferred to downstream waters and eventually reach the coastal zones, where they may
45 induce harmful algal blooms or cause hypoxia along coastlines (He and Xu, 2015; Beusen et al., 2016; Le Moal et al., 2019).
46 Hence, it is of pivotal importance to understand N and P dynamics in the urban freshwater bodies in order to mitigate the input
47 of nutrients into the oceans (e.g. Nyenje, et al., 2010; Toor et al., Paerl et al., 2016; 2017; Le Moal et al., 2019).

48 Nutrients dynamics are governed by biological, chemical and physical processes and their interactions. Assimilation by
49 primary producers is a major biological factor regulating N and P concentrations in the aquatic environment. Aquatic micro-
50 and macro-organisms assimilate P as PO_4 and N mainly in fixed forms such as nitrate (NO_3) and ammonium (NH_4), but for
51 some specific organisms also in the form of N_2 . NH_4 is the preferred N-form by microbes in some cases like in estuaries
52 (Middelburg and Nieuwenhuize, 2000), but the uptake rate for both NH_4 and NO_3 can achieve maximum rates under sustained
53 exposure of NH_4 or NO_3 (Bunch and Bernot, 2012). Moreover, the nitrogen species are also involved in redox transformations
54 (Soetaert and Herman, 1995). Under anaerobic conditions, NO_3 can be reduced to NH_4 , in particular with high organic matter
55 contents, or denitrified to N_2 and N_2O (Mulder et al., 1995), the latter is a climate-active gas. Under aerobic conditions, NH_4
56 can be oxidized to NO_3 through nitrification by nitrifying microbes, which is an O_2 consuming and acid generating process.
57 Nitrification even occurs under cold conditions (below 10 °C) (Painter, 1970; Wilczak et al., 1996; Cavaliere and Baulch,
58 2019).

59 The mixing of water from different flow routes is an important hydrological process that controls nutrient dynamics
60 (Rozemeijer and Broers, 2007; Rozemeijer et al., 2010a; Van der Grift et al., 2014; Yu et al., 2019). As nutrient concentrations
61 and speciation differ among different flow routes (Wriedt et al., 2007; Rozemeijer et al., 2010a; Yu et al., 2019; Yang and
62 Toor, 2019), the mixing process results in dilution or enrichment of nutrients in surface water bodies during precipitation
63 events (Wang et al., 2016).

64 Retention is another factor that determines nutrient concentrations and transport (McGlathery et al., 2001; Zhu et al., 2004;
65 Henry and Fisher, 2003), especially for phosphorus most of which is retained in inland water bodies sediment (Audet et al.,
66 2019). The retained P are either being permanently buried in the sediment or temporarily stored and acting later on as internal
67 nutrient source (Kleeberg et al., 2007; Filippelli, 2008; Zhang et al., 2018). Multiple researchers have highlighted the influence
68 of iron chemistry on the dynamics of P in pH neutral environments (Chen et al., 2018; Van der Grift et al., 2018). This is
69 especially relevant when iron-rich groundwater interacts with surface water (Griffioen, 2006; Rozemeijer et al., 2010a; Van
70 der Grift, 2014; Yu et al., 2019), in which P is immobilized by the formation of iron(oxy)hydroxides during groundwater
71 aeration. However, changes in chemistry or temperature may lead to the release of P and reduced iron. For instance, under
72 anaerobic conditions, Fe and P can be mobilized by sulfate reduction, but this can be counteracted by the presence of NO_3 as
73 electron acceptor (Smolders et al., 2006).

74 Most studies of eutrophication are based on discrete sampling events which can give a general pattern of nutrient dynamics,
75 but can easily miss important nutrient transport and processing phenomena (Rozemeijer et al., 2010; Rode et al., 2016; Toor
76 et al., 2017). The countermeasures to control eutrophication have been hampered because of limited knowledge of N and P
77 dynamics, for instance their response to changing weather conditions and land use (van Geer et al., 2016). In the past few years,
78 the development of new sensors and sampling technologies allow us to obtain data with substantially shorter intervals. In this
79 paper, the high frequency monitoring technology is referred to as an automatic monitoring program with sampling and
80 analyzing frequencies that are sufficient for obtaining detailed water quality variation information. High frequency technology
81 has proved to be a way to understand nutrient dynamics (Rode et al., 2016; Van Geer et al., 2016; Bieroza et al., 2018). Due
82 to the abundant information offered by this technology, combined methodologies have been developed to quantitatively
83 understand the in stream hydrochemistry of nutrients (Miller et al., 2016, Van der Grift et al., 2016, Duncan et al., 2017).

84 In our previous study on the water quality of Amsterdam (Yu et al., 2019), the transport routes of N and P from groundwater
 85 to surface water through seepage and drains were identified. In addition, spatial and temporal concentration patterns from
 86 discrete sampling campaigns showed a clear dilution pattern of other water quality parameters such as EC. However, the
 87 temporal patterns of N and P were still poorly understood, probably due to their reactive nature and more complex
 88 biogeochemistry. In order to obtain insight into the controlling mechanisms of N and P transport and fate in urban delta
 89 catchments affected by groundwater, we performed a year-round high-resolution N and P concentration monitoring campaign.
 90 A deep understanding of the water quality dynamic drivers would be a great asset for controlling eutrophication and improving
 91 aquatic ecological status (Fletcher et al., 2015; Díaz et al., 2016; Eggimann et al., 2017; Nizzoli et al., 2020). We conducted a
 92 one-year high frequency monitoring campaign in 2016-2017. Measured parameters were EC, NH₄, TP, turbidity and water
 93 temperature. The temporal patterns of these parameters were studied at three time scales: the annual scale, rain event scale,
 94 and pumping event scale.

95 2 Methods

96 2.1 Study site

97 The Geuzenveld study site is part of an urban lowland polder catchment, which is characterized by groundwater seepage that
 98 constantly determines the surface water quality, being the main source of solutes in the water system. The groundwater seepage
 99 is a continuous source of anoxic, iron and nutrient rich slightly brackish waters. Yu et al. 2019) presented the results of a 10
 100 year monitoring program describing the main processes determining the water quality in the catchments, which is dominated
 101 by mixing of runoff water and seepage water. A high-frequency monitoring campaign was set-up to further unravel the
 102 temporal pattern on the nutrient N and P, of which N is typically present in the form of NH₄ from groundwater.

103 Geuzenveld is a newly built urban polder on the west of the city of Amsterdam (Fig.1). Since 1990s, when it was converted
 104 from agricultural to urban land, it has developed into a highly paved area. Similar to other new neighborhoods, Geuzenveld is
 105 equipped with a separated drainage system. A rain harvesting system was installed on all the buildings and houses in the polder,
 106 leading rain water from the roof and the street directly to the ditches, which results in fast and large amounts of runoff during
 107 storm events. Geuzenveld is a groundwater fed catchment due to the constantly higher groundwater head (-2.5 ~ -3 m NAP)
 108 in the main aquifer relative to the surface water level in the polder ditches (~ -4.25 m NAP). (Fig.2). To keep the foundations
 109 of the building dry, there is a groundwater drainage system placed under an artificial sandy layer, right on top of a natural clay
 110 layer. The drain elevations range from -4.84 to -4.61 m NAP, which is below the phreatic groundwater level throughout the
 111 year, making sure that groundwater seepage either discharges through the drains or the ditches.

112 The water system of Geuzenveld is connected to the secondary water channel to its east, then connected to the adjacent primary
 113 channel, called boezem, the Boezem Haarlemmerweg. The boezem water level is -2.10 m NAP. It is much higher than the
 114 target surface water level of Geuzenveld, -4.25 m NAP. The surface water level in polder Geuzenveld is controlled by a pump
 115 station, which is the main outlet of this polder, situated in the northeastern corner.

116 There are two pumps (Pump 1 and Pump 2) in the pumping station, and they have different start and end pumping threshold
 117 points (Table 1).

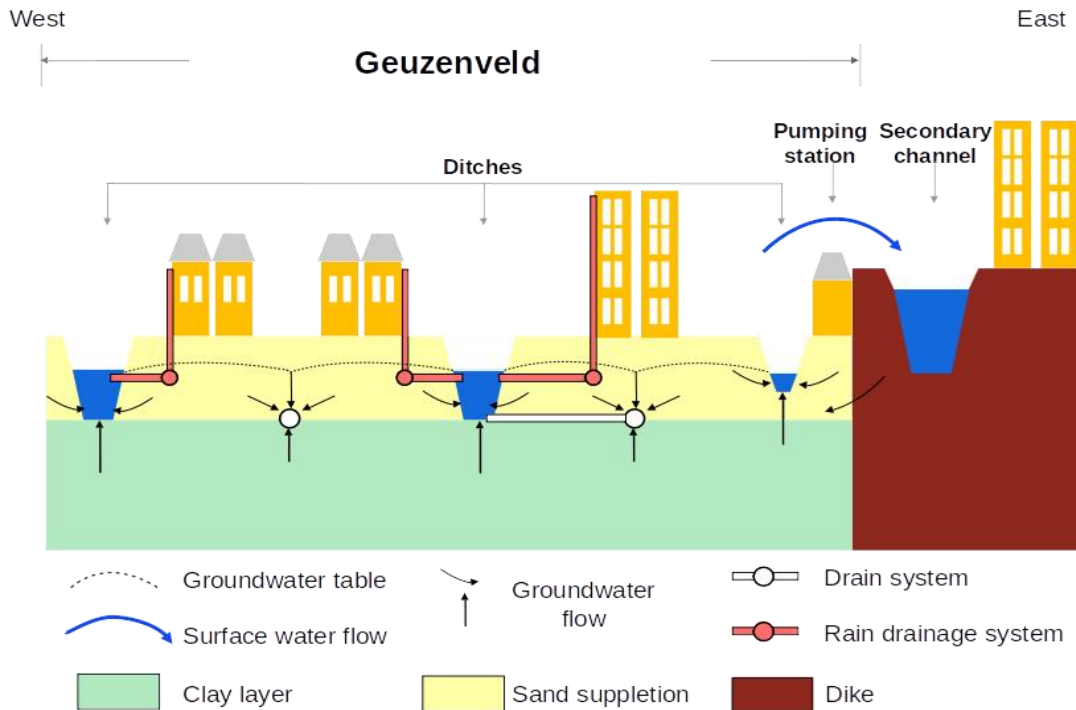
118 **Table 1 Pumping scheme of polder Geuzenveld**

Time	Settings	Pump 1	Pump 2
05:00:00-19:00:00	Start point (m NAP)	-4.20	-4.16
	End point (m NAP)	-4.26	-4.24
19:00:00-05:00:00	Start point (m NAP)	-4.23	-4.18
	End point (m NAP)	-4.31	-4.29

119

120
121
122
123
124
125
126

The two pumps are activated when the surface water level exceeds the triggering level which are furthermore separated as day and night triggering levels (Table 1). The capacity of each pump is 3.6 m³ per minute. Most of the time, only one of the two pumps works and the surface water level is maintained between -4.31 m NAP and -4.23 m NAP, which are the night inactive and active pumping levels respectively. Normally, the surface water level drops immediately when the pump(s) start(s) working. Once the pump(s) stop(s), the surface water level will steadily rise due to the continuous inflow of groundwater seepage. During rainfall events, the surface water level rises faster (Fig.2A).



127



128
129
130

Figure 1 Location of polder Geuzenveld (source: © Google Maps) and its landscape cross section and rain water and groundwater drainage system

131 2.2 Monitoring network setup

132 2.2.1 High frequency monitoring

133 A high frequency monitoring network was built on a temporary floating platform in front of the pumping station. The water
134 flowed around and underneath this platform to the pumping station when the pumps started working. One year time series of
135 $\text{NH}_4\text{-N}$ (mg L^{-1}), TP (and ortho-P) (mg L^{-1}), turbidity (Formazin Nephelometric Unit, FNU), electrical conductivity (EC, $\mu\text{S/cm}$)
136 and water temperature ($^{\circ}\text{C}$) were collected by the following equipment: a Sigmatax sampler combined with a Phosphax sigma
137 auto analyser for total phosphorus (TP), Amtax for $\text{NH}_4\text{-N}$ combined with a Filtrax automatic sampler, a Solitax-tline sc for
138 turbidity (manufactured by: Hach Lange GmbH Düsseldorf, Germany), and CTD-Diver for electrical conductivity (EC) and
139 water temperature (manufactured by: Van Essen Instruments, Delft, The Netherlands). The monitoring frequencies were set
140 to 20 mins, 10 mins, 5 mins, 5 mins and 5 mins interval for TP, $\text{NH}_4\text{-N}$, turbidity, EC and water temperature, respectively.

141 The Phosphax sigma is an analogue analyser for the high precision determination of total phosphorus concentration in
142 accordance with EN 1189 Phosphormolybdenum Blue method. Samples are automatically taken through a Sigmatax sampling
143 probe and include suspended solids. Subsequently, the sample is ultrasonic homogenized before delivery to the Phosphax
144 sigma. It is digested by the sulphuric acid-persulphate method (APHA/WWA-WPCF, 1989), and analysed with a LED
145 photometer (at 880 nm) (Hach, user manual of Phosphax sigma, 2016).

146 Samples for NH_4 are prepared by a filtration system, Filtrax. It continuously extracts samples through two ultra-filtration
147 membranes ($0.15\ \mu\text{m}$) plates. Particles get dispersed by a continuous aeration system near the surface of the membranes (The
148 aeration caused severe build-up iron precipitates on the plates). The samples are then delivered to Amtax sc for analysis. The
149 ammonium in the sample is first converted to gaseous ammonia. Only the NH_3 gas passes through the gas-permeable membrane
150 of the electrode and is detected. This method guarantees a wide measuring range and is less sensitive to other compounds
151 compared to methods that make use of an ion-selective electrode (ISE). The Amtax sc in our study was calibrated automatically
152 at 22:00 every 24 hours before September 2016, every 48 hours thereafter. Maintenance work was conducted weekly as the
153 tubes were easily blocked by iron precipitates (Hach, user manual of Amtax sc, 2013).

154 The Solitax-tline sc sensor is a turbidity sensor with dual-beam optics and added backscatter. The measuring principle is based
155 on a combined infrared absorption scattered light technique that measures the lowest turbidity values in accordance with DIN
156 EN 27027 just as precisely and continuously as high sludge contents. Using this method, the light scattered sideways by the
157 turbidity particles is measured over an angle of 90° (Hach, User manual of Solitax sc, 2009).

158 The monitoring period of NH_4 and turbidity is from 2016-05-10 to 2017-06-16. Time series of phosphorus were obtained from
159 2016-05-23 to 2017-06-16. Electrical conductivity and temperature data are from 2016-06-10 to 2017-06-15. The NO_3 analyser,
160 Nitratax, time series consistently showed an artificial drift and proved to be unreliable in our field setting, possibly due to
161 biofilm accumulation in combination with iron oxides precipitation (see discussion). All the equipment outputs were integrated
162 into one wireless station. The monitoring station was shut down several times by lightning, so an electricity restart program
163 was also applied in this network. It worked for all equipment except for the Phosphax, which had to be restarted manually after
164 a black out.

165 Precipitation (hourly) and Evapotranspiration (daily) data were downloaded from the Schiphol KNMI station which is about
166 2 km away from Geuzenveld. Hourly pumping activity and surface water level data were obtained from Waternet, the water
167 authority of Amsterdam.

168 2.2.2 Low frequency monitoring

169 Since 2006, Waternet has monitored the water quality with a frequency of 12 times per year by sampling at the pumping station
170 of Geuzenveld. Between 2016 and 2017, the sampling frequency was increased to twice per month. We selected the following
171 parameters from the routine monitoring campaign: (1) EC, $\text{NH}_4\text{-N}$ and TP to fill in the gaps in the continuous time series, and

172 to verify and monitor the potential drift and offset of the high frequency data and (2) pH, O₂, HCO₃, NO₃, TN, Kjeldahl-N,
 173 suspended solids (detail of methods are described by Yu et al, 2019), chlorophyll-a, and transparency for further understanding
 174 the biogeochemical processes. Organic-N was estimated by subtracting NH₄-N from Kjeldahl-N.
 175 Bi-weekly total iron in the water column was analysed separately using ICP-AES (inductively coupled plasma-atomic emission
 176 spectrometry). Total Fe was analysed from samples to which HgCl₂ was added for preservation and that were stored in a dark
 177 and cool environment. To release all Fe that may have sorbed or precipitated during storage, we added 1 or 0.5 ml HCl in the
 178 water samples to dissolve eventual flocks. Then the samples were homogenized in an ultrasonic bath for 24h, mixed again to
 179 break down all the flocks. For extraction of all the Fe, we transferred 10 mL of the homogenized sample into a Teflon bottle,
 180 added 3.2 mL HCl : HNO₃ 3:1 , and stored in a stove at 90 °C for 24 hours. The final solutions were analysed by ICP-AES.
 181 Blanks were included and treated identical to samples.

182 2.3 Data processing and analysis

183 A correlation analysis between the high frequency and discrete monitoring data was applied to illustrate the reliability of the
 184 high frequency time series. Furthermore, the time series data were analysed at 3 time scales: annual scale, rainfall events
 185 (several days) and single pumping events (several hours). The relationships among the monitored parameters was explored by
 186 testing their correlations at each time scale. At the annual scale, a correlation analysis was applied to the complete time period
 187 and the wet and dry periods (definition in section 3.1.1). To discern the hydrological and chemical/biological attributes to the
 188 observed dynamics, a linear mixing model was introduced at the annual scale, assuming precipitation and groundwater seepage
 189 are the only water inputs, pumping and evapotranspiration are the only outputs, and pumping activity is the only way solutes
 190 leave the water system. In this model, we assumed a constant seepage rate. Accordingly, surface water level was calculated
 191 from:

$$193 \frac{dV}{dt} = (P(t) + S - E(t)) * A_{polder} - Pump(t) \quad (1)$$

$$194 L(t) = V(t) / A_{ditch} \quad (2)$$

196 V is total water volume in the ditches, P is precipitation, S is a constant seepage, E is potential evapotranspiration, A_{polder} is
 197 area of the polder, $Pump(t)$ is water volume being pumped out with maximum capacity 216 m³ h⁻¹, A_{ditch} the area of the ditches
 198 in the polder. L is surface water level in the ditches. Water level L determines the activation of pumping activity. Once $L(t)$
 199 exceeds the upper ranges of water level (start point, section 2.1), the pumps will start to pump until L goes below the stopping
 200 end (section 2.1) in the pumping scheme. Given the year-round seepage conditions throughout the polder, combined with an
 201 artificially drained subsurface, we assumed that the potential evapotranspiration was close to the actual evapotranspiration
 202 as no water shortages occur in our situation. In this study, we used the difference between groundwater head in the first
 203 aquifer and the surface water level (Figure 2A) to estimate a range of the seepage. The actual number of 2 mm per day was
 204 chosen based on the behavior of the mixing model and calibrated using the measured surface water levels (Figure S1).

205 A complete mixing of solutes was assumed in the model, which means that seepage, ditch water and precipitation mix
 206 instantaneously when they enter the surface water. A delay from precipitation to run-off/drainage and to ditches was not
 207 specifically considered.

$$209 \frac{d(VC)}{dt} = S * A_{polder} * C_{gw} + P(t) * A_{polder} * C_P - Pump(t) * C(t) \quad (3)$$

210

211 *V* is the ditch water volume given by equation (1), $C(t)$ is solute concentration at time t , C_{gw} is the average groundwater
212 concentration, C_p is the average concentration in runoff.

213 In our study area, the EC is a useful water quality parameter for describing the mixing processes between groundwater and
214 runoff water, as the EC represents the end members of the mixing: groundwater with a high EC (1750 $\mu\text{S}/\text{cm}$) and runoff
215 water (100 $\mu\text{S}/\text{cm}$) with a low EC (see also Yu et al., 2019). Moreover, we assume that EC behaving as a conservative tracer
216 as the EC is highly correlated with the Cl concentration ($R^2 = 0.71$, p -value < 0.05) and the temporal patterns of EC and Cl are
217 very similar (see supplement Figure S2). In the model, seepage rate was adapted to get the best fit between the modeled and
218 the measured EC. The calibrated seepage rate was 2.0 mm d^{-1} . Compared to EC, nutrients are highly reactive solutes and thus
219 can vary a lot along their flow routes due to biogeochemical processes. The model provided a tool to simulate concentration
220 dynamics under the assumption that EC, NH_4 and TP were conservative. The simulated concentrations of EC, NH_4 -N and TP
221 were plotted together with the high frequency measured time series. A comparison between the modeled and the measured
222 results was performed by using correlation analysis.

223 The average concentration of EC in groundwater was set equal to the average of the sampling survey, which was 1750 $\mu\text{S}/\text{cm}$
224 (including both deep and shallow groundwater, Yu et al., 2019). For the NH_4 and TP concentration data, we chose the
225 measurement from a drain sampling point (Drain 3, Yu et al., 2019) in the middle of the polder as the non-disturbed
226 groundwater collected by the drains in this area of the polder. They were 8.1 mg N L^{-1} and 1.6 mg L^{-1} respectively. The starting
227 (01-06-2015) concentrations were 1200 $\mu\text{S}/\text{cm}$, 4 mg L^{-1} , and 2 mg L^{-1} for EC, NH_4 , and TP respectively. The model was not
228 sensitive to the selected end-member values.

229 The time series data were further analysed at shorter scales: rain event scale and pumping event scale. Four rain events were
230 selected according to the dilution extent of EC, defined as an EC value reduced by over 35%, they were: 10-06-2016 ~ 15-07-
231 2016, 15-08-2016 ~ 26-09-2016, 10-11-2016 ~ 05-01-2017, and 20-02-2017 ~ 10-04-2017. These four events covered both
232 EC dilution during rainfall and the recovery afterwards in different seasons. We selected 4 representative pumping events to
233 present the response of EC, NH_4 , TP, and turbidity to the pumping activities. Those events were in 15-07-2016 ~ 17-07-2016,
234 27-10-2016 ~ 29-10-2016, 20-12-2016 ~ 22-12-2016, and 05-05-2017 ~ 07-05-2017. Correlation analysis was as well applied
235 to each event at the corresponding two time scales, averaging over whole days for precipitation events and over hours for
236 pumping events. Data processing and analyzing were performed using Rstudio (R version 4.0.2) and time series package “xts”.

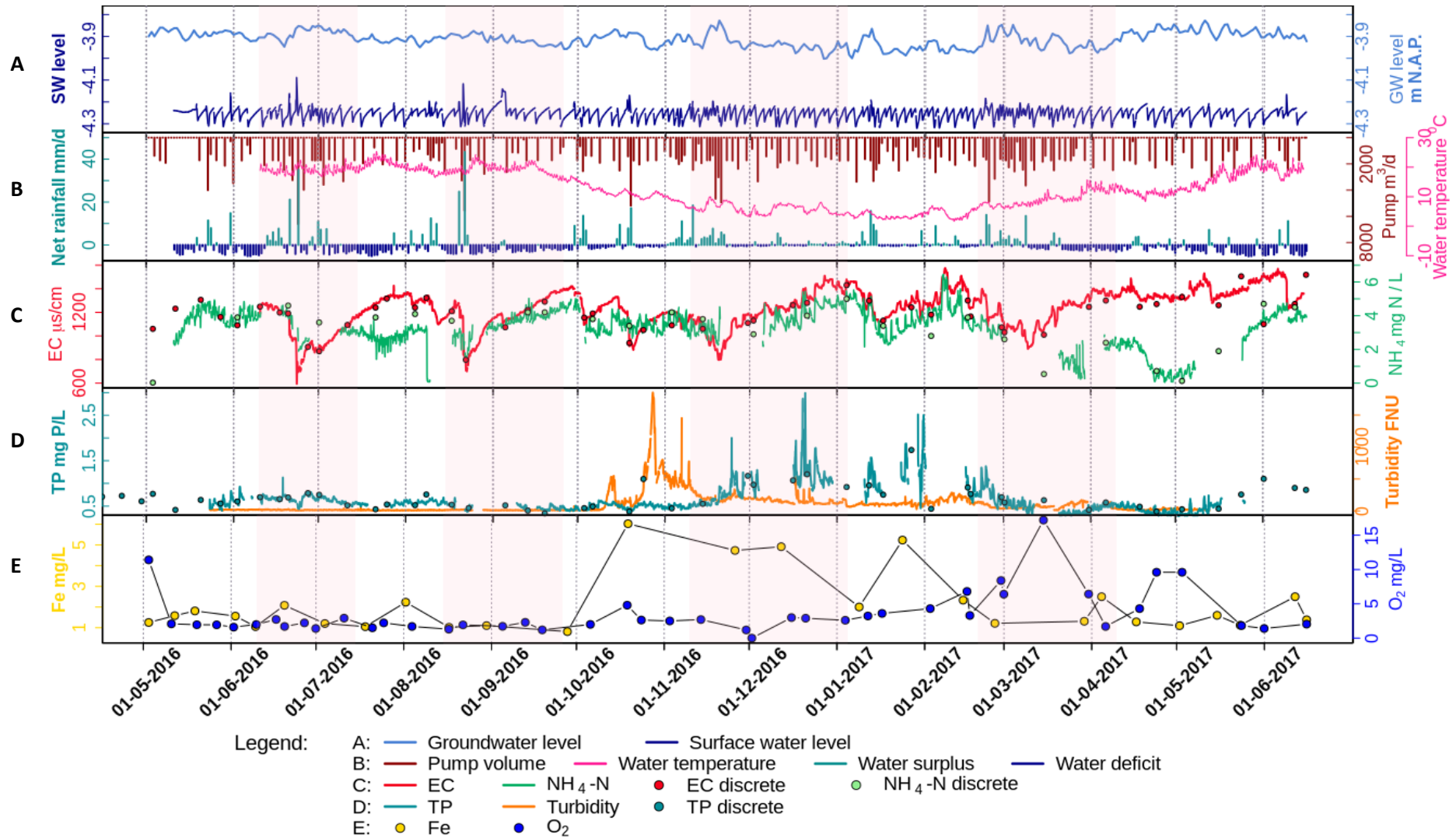
237 **3. Results**

238 **3.1 Annual pattern of meteorological, hydrological, and water quality time series**

239 **3.1.1 Meteorological and hydrological conditions in polder Geuzenveld**

240 To explain the time series (Fig. 2), we distinguish between dry/wet periods and dry/wet seasons. The wet and dry periods (days
241 to weeks) are represented by a water surplus (light blue color in Fig.2B, daily evapotranspiration $<$ daily precipitation) or a
242 water deficiency (dark blue in Fig.2B, daily evapotranspiration $>$ daily precipitation). We defined the wet and dry seasons
243 based on water surplus and deficit. The average net rainfall (the water surplus/deficit in Figure 2) is 1.4 mm/d for the period
244 of 01-10-2016~15-03-2017, and -0.8 mm/d for the rest. Subsequently, we statistically analysed the difference between these
245 two periods for multiple parameters. Table 2 shows the mean of each parameter for the wet and dry seasons. The wet and dry
246 seasons means are significant different for all parameters, but the EC.

247



248
249
250
251
252
253

Figure 2 Time series of (A) surface water level (SW level) and groundwater level (m NAP), (B) net rainfall (daily water surplus (+) (lightblue) and deficit (-) (darkblue), mm d⁻¹) and daily pumping volume (Pump m³ d⁻¹), (C) hourly time series of EC ($\mu\text{S/cm}$) and NH₄-N (mg N L⁻¹), and (D) hourly TP, turbidity, (E) discrete samples of Fe (total iron in water column) and O₂ concentrations (mg L⁻¹). The dots in (C) and (D) are the corresponding discrete sampling data, which are plotted to show their close match to the continuous time series data, as well as to fill in the gaps. All data were monitored at the pump station. The transparent pink blocks are the selected rain events for further analysis in section 3.3.

Table 2 The mean of each parameter, and the significance for the wet and dry seasons

	Net rainfall* mm/d	Pump volume* m ³ /d	Water temperature* °C	EC µs/cm	NH ₄ * mg N/L	TP * mg P/L	Turbidity* FNU	Fe* mg/L	O ₂ * mg/L
Wet	1.4	1050	6.7	1212	3.7	0.8	197	3.4	4.3
dry	-0.8	712	17	1252	3.0	0.5	15	1.5	3.3

255 * $p < 0.05$

256

257 Over the whole monitoring period, the water temperature ranged between 2 to 26 °C. From June to mid-September 2016, the
258 temperature remained above 18 °C, then declined to become lower than 10 °C at the end of October. The following four months
259 (November to February) were the coldest. Especially in January and February 2017, during which the water temperature
260 dropped to below 3 °C. By the end of February temperatures started to rise again to reach 10 °C by the end of March 2017.

261 The surface water level in Geuzenveld has been maintained between -4.31 and -4.1 m NAP, strictly regulated by pumping
262 (Fig.2A). After the pumps stopped, the surface water level recovered faster during the wet season (between October 2016 and
263 March 2017) than during the dry season. Similarly, the shallow groundwater level positively corresponded to the precipitation
264 and negatively to the daily accumulative pumping volume. The phreatic groundwater level in Fig.2A (light blue) was from
265 one of the piezometers, which lies right outside of the polder (Figure 1, 52°22'46.0"N 4°47'15.6"E). In contrast to the constant
266 surface water levels (Fig.2A, dark blue), the shallow groundwater had relatively low levels in the wet season compared to the
267 dry season. This is related to the water level regulation of the boezem Haarlemmerweg with higher levels in summer than in
268 winter (<https://www.rijnland.net/actueel/water-en-weer/waterpeil>). Phreatic water levels were consistently 20-40 cm higher
269 than the surface water level in the polder, which confirms the continuous groundwater seepage into the surface water system.

270 3.1.2 Annual water quality patterns

271 The coefficients of determination (R^2 “Pearson” method used) between the high frequency data and the routine discrete
272 sampling data from the water authority are 0.88 for EC (p -value < 0.05), 0.92 for NH₄ (p -value < 0.05), and 0.97 for TP (p -
273 value < 0.05). The scatter plots between the high and low frequency measurements are shown in Figure S7.

274 During a rainfall event, rain and runoff from pavements and roofs, which were collected by a separate drainage system, directly
275 fed the surface water (Fig.1). Distinct rainfall events cause a strong dilution pattern of both EC and NH₄ (in Fig.2C). The EC
276 ranged from 600 to 1500 µS/cm. In general, during rainfall events, the EC declined because of dilution, while, after the events,
277 EC gradually rose back up to around 1500 µS/cm. The duration of this process, i.e. *recovery time*, was longer in the wet season
278 than in the dry season. A similar pattern of dilution and recovery is also visible for NH₄, especially for the period August 2016
279 – March 2017, where NH₄ shows a very similar response as EC (Table S2, wet season, $R^2 = 0.73$), although with somewhat
280 larger day to day fluctuations. However, a contrasting pattern without NH₄ recovery occurred twice: from the middle of June
281 to the end of August 2016 and from the middle of March to the middle of May 2017. During these periods, concentrations of
282 NH₄ were considerably lower and deviated from the slope of the EC pattern. NH₄ decreased from around 4 mg L⁻¹ to around
283 2 mg L⁻¹ between the middle of June to the end of August 2016, but the continuous NH₄ measurements are not supported by
284 the discrete samples which follow the EC pattern more closely. During the second period from March to the middle of May
285 the deviation from the recovery pattern is more pronounced, and NH₄ concentrations dropped to almost 0 mg L⁻¹ and started
286 recovering from the beginning of May. This pattern is fully supported by the available discrete samples. During the same
287 period in 2016 the high-frequency monitoring had not yet started, a single NH₄ discrete measurement is available for the 2nd
288 of May, that seems to reveal a similar pattern in the spring of 2016.

289 Both TP and turbidity showed contrasting patterns during the wet and dry seasons (Fig. 2D). Turbidity stayed below 60 FNU
290 during the dry season until October and rapidly increased after a first rain event to 500 FNU (more details refer to Figure S3

291 in supplementary information). A drop to about 200 FNU occurred right after this first peak, which seemed to correspond to
292 excessive precipitation and a large pumping volume (Fig.2B). Soon after, turbidity went up again and peaked at 1800 FNU.
293 Turbidity leveled off towards values around 200 FNU for the rest of the wet season and dropped below 60 FNU from April
294 2017 onwards.

295 TP concentrations were significantly higher during the period between 15-11-2016 and 01-03-2017 than the rest of the time
296 (p -value < 0.001 , Figure S5), during which TP fluctuated around 0.5 mg L^{-1} , but always below 1 mg L^{-1} . During the wet season
297 with the low temperatures (Table S2, $R^2 = -0.68$), TP almost constantly stayed above 1 mg L^{-1} and even reached values of
298 about 3 mg L^{-1} in December. Although there were large gaps in the TP time series during this period, the high TP concentrations
299 appear to have been diluted by rain events, for example the event at around January 10th, 2017. Most discrete samples
300 measurements of TP matched well with values from the high frequency time series (Fig.2D, Table S1, $R^2 = 0.88$).

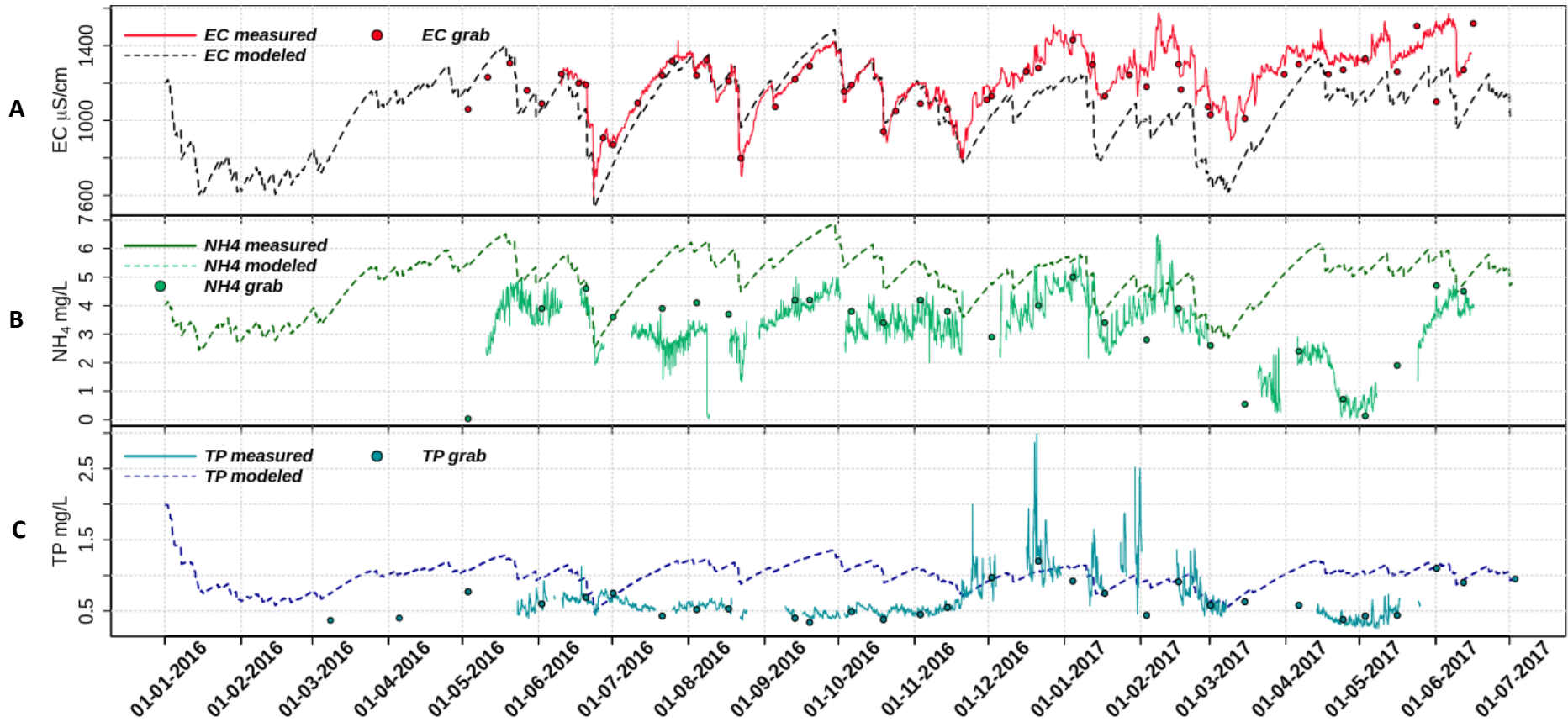
301 Total-Fe concentrations were most of time lower than 2 mg L^{-1} (Fig. 2E), but for the wet season concentrations were higher
302 and reached up to about 6 mg L^{-1} . The initiation of Fe increases at the beginning of the wet season coincided with that of
303 turbidity (Fig.2D and Table S2, $R^2 = 0.72$). Upon the increasing temperature in March 2017, total Fe concentrations dropped
304 back to below 2 mg L^{-1} (a negative correlation between temperature and Fe is shown in Table S1). Dissolved O_2 concentrations
305 were generally low in the water column; i.e. usually below 5 mg L^{-1} . Concentrations of over 3 mg L^{-1} were only found in
306 March, April and May.

307 **3.2 Model of water quality time series based on water balance**

308 A simple fixed-end-member mixing model was used to reconstruct the conservative mixing of EC, NH_4 , and TP. The simulated
309 and the measured EC, NH_4 , and TP are plotted in Figure 3. The correlations between the modeled and measured results are
310 shown in the supplementary information (Table S4-S6). Potential processes that might deprive or enrich nutrients relative to
311 the conservative mixing process along the flow routes were inferred from the discrepancies between the modeled and the
312 measured data. Figure 3(A) and Table S5 show that the predicted and observed EC dynamics agree reasonably well from May
313 to November 20th, 2016 ($R^2 = 0.91$). After that, the conservative mixing approach underestimated the EC but the main dynamics
314 and the amplitudes were still reproduced (Table S6, $R^2 = 0.82$); as groundwater is the only contributor to the high EC due to
315 the seepage of quite mineralized, slightly brackish water, the model must underestimate the seepage flux from November 20th,
316 2016 on. Overall, the observed dynamics of EC are consistent with mixing of high EC seepage water with low EC runoff water
317 (coefficient of determination between the modeled and measured EC is 0.65 over the complete period, Table S4).

318 The dynamics of measured NH_4 concentrations show close resemblance to the model results, especially during the wet season
319 (01-10-2016~15-03-2017). Clearly, NH_4 is diluted during the rain events and a gradual increase of NH_4 starts after each rain
320 event during the wet season showing slopes that resemble the model reconstruction. Over the whole period, measured NH_4
321 concentrations were overestimated by the model, indicating that some NH_4 is probably lost due to non-conservative processes.
322 This is especially true for the spring season of 2017, where NH_4 concentrations must be controlled by additional processes.
323 Concentrations of TP are generally far below the conservative model reconstruction, except between the end of November and
324 the beginning of March. During this particular period the minimum measured TP concentrations are captured nicely by the
325 conservative model, however distinct peaks up to 3 mg L^{-1} are not captured by the model and must have different physical or
326 chemical processes determining them.

327
328
329
330
331
332



333
 334
 335
 336

Figure 3 Plots of fixed-end-member mixing model predicted (A) EC, (B) NH_4 and (C) TP with their measured time series data and the discrete sampling results.

337 3.3 Water quality responses to single events analysis

338 To elucidate the response pattern of water quality to precipitation and pumping activity, we selected four major events (Fig.2
339 (4 pink shades) and Figure 4) and four pumping events (Figure 5). The former events were chosen according to their clear
340 dilution pattern of EC (Fig.4), while the latter were pumping events without occurrence of rainfall (Fig.5). All seasons were
341 covered, including some of the wet and dry periods.

342 3.3.1 Rainfall events

343 EC and NH₄ showed clear dilution and recovery patterns during all events, while the pattern was not clear for TP and turbidity
344 (Fig.4). The extent of dilution of EC appears to depend on the precipitation intensity. Rainfall during the recovery period
345 determined how long it took to recover back to the highest level. The short but intensive rainfall during dry season events 1
346 and 2 reduced EC rapidly from around 1300 to around 700 $\mu\text{S}/\text{cm}$, while the recovery took about 1 month. Events 3 and 4 had
347 less rainfall and dilution of EC was less (from about 1300 to about 800 $\mu\text{S}/\text{cm}$) and recovery took more than one and a half
348 month in event 3, during which multiple small events occurred. The dilution patterns of the NH₄ in events 1 and 2 were similar
349 to those of EC ($R^2 = 0.86$ and 0.83 , respectively, Table S7 & S8) and show resemblance for event 3 ($R^2 = 0.75$, Table S10).
350 Moreover, a direct negative correlation between NH₄ and rain intensity supports this dilution effect for event 2. Due to the data
351 gaps of NH₄ in event 4 we cannot completely describe the pattern of NH₄ for this one, but it corresponds with that start of
352 reduced NH₄ which was described in sections 3.1 and 3.2.

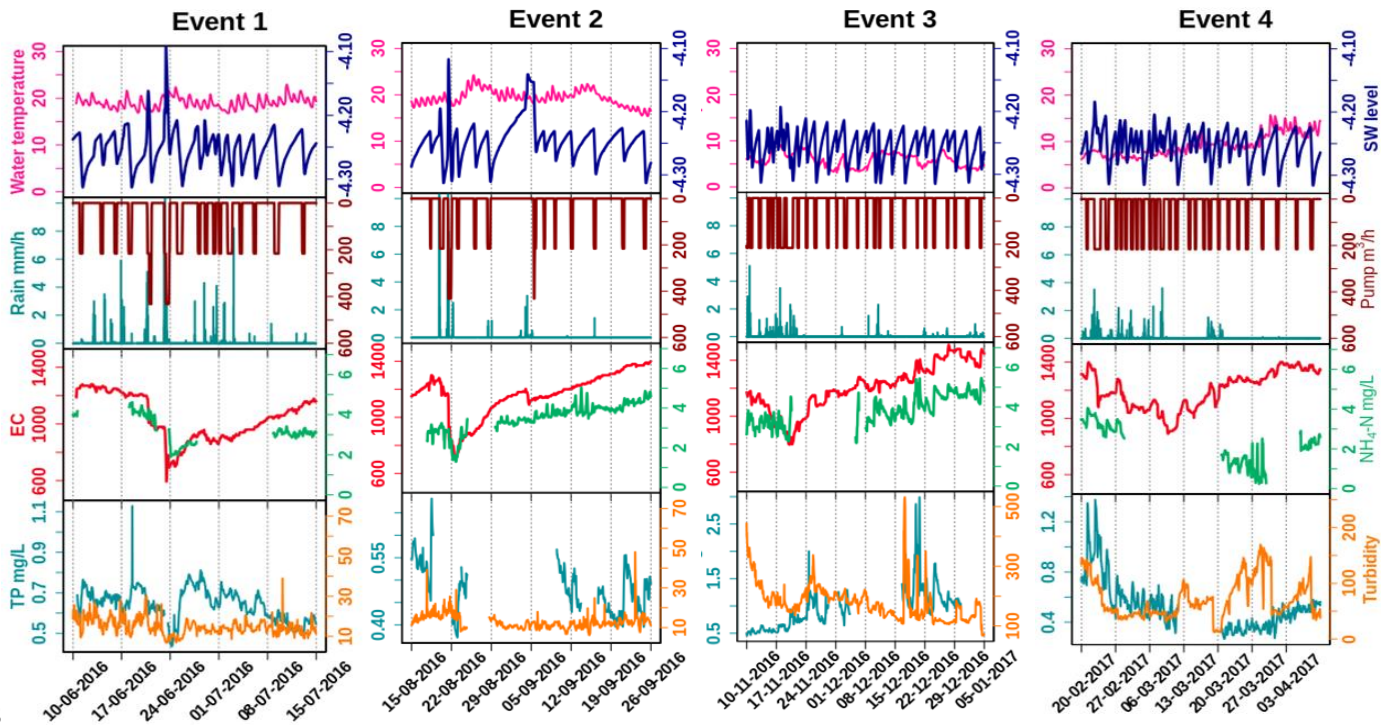
353 The response of TP was generally not related to the intensity of rainfall and pumping, except for event 3 during the wet period.
354 Dilution effects, as were observed for NH₄, were not observed for TP for events 1, 2 and 4. During the wet season event 3, TP
355 concentrations show negative correlations with precipitation and pumping intensity ($R^2 = -0.79$ and -0.59 , respectively, Table
356 S9) and correspond with decreasing turbidity. Event 4 marks the transition between the wet and dry season and the drop in TP
357 coincides with the drop in NH₄, independently from individual rain storms during the dry season.

358 During the dry season (with event 1 and 2 included) turbidity always stayed below 50 FNU. Turbidity sometimes showed
359 single peaks which are likely related to disturbances of the floating platform by wind and should probably be treated as false
360 signals. Turbidity is more variable and has higher variance for wet season events 3 and 4, which corresponds with the findings
361 of the annual scale analysis (section 3.1.2). During event 3, turbidity varied between 100 and 500 FNU. Although clear relations
362 exist between Fe, TP and turbidity, all higher during the wet season (Figure 2, Table S2), these are not clearly reflected at the
363 scale of individual precipitation events. Simultaneous peaks of TP and turbidity occur that are not easily related to the weather
364 conditions in November and December but TP and turbidity show contrasting signals at the start of the event. The turbidity
365 clearly decreases during rain storm event 3 and at the start of event 4. This change is not reflected by the correlation at the total
366 event scale (Tables S9 and S10) but obvious when studying only the time scale of the decreasing limb of the EC dilution.
367 Event 4 coincides with the transition to the spring season in 2017, showing decreasing EC, TP and turbidity in the last rains of
368 the wet season and a strong decrease of NH₄ and increase of turbidity when conditions dried up and temperatures rose.

369 3.3.2 Pumping events and day and night pattern

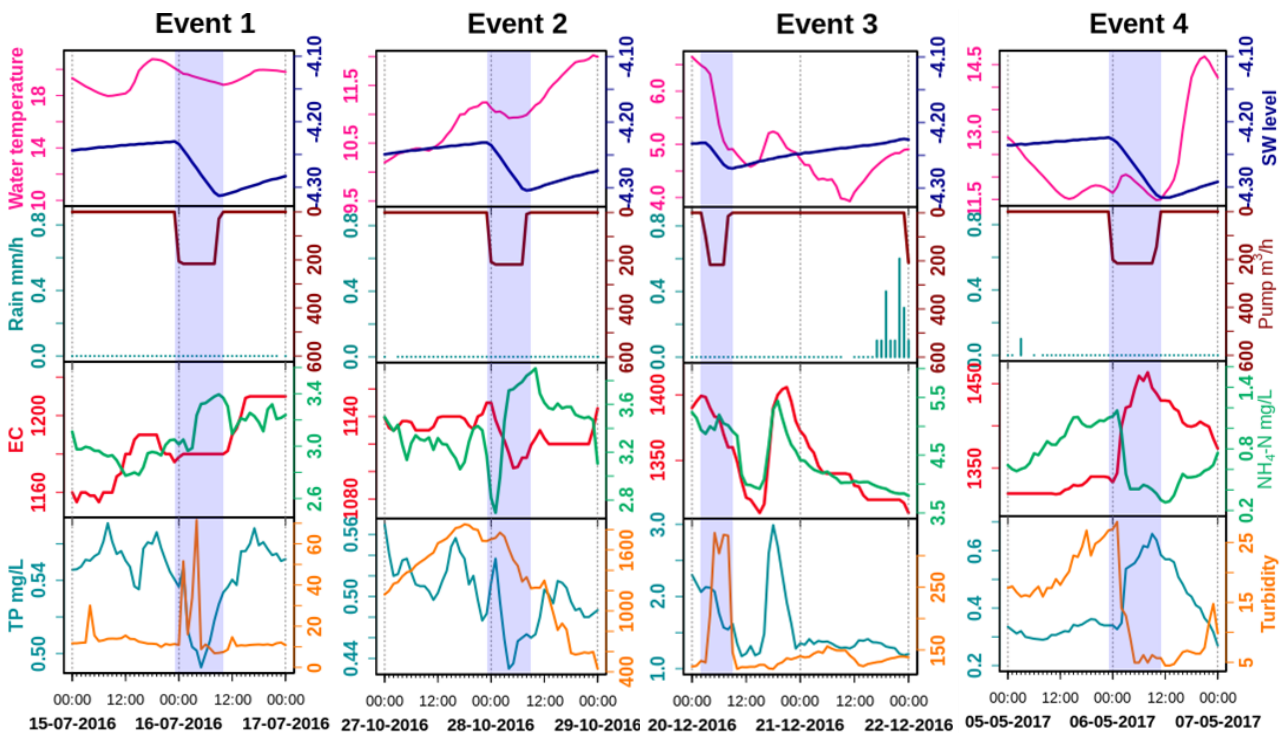
370 The selected pumping events covered four seasons: summer (2016 July, event 1), autumn (2016 October, late autumn, event
371 2), winter (2016 December, event 3) and spring (2017 May, event 4) (Fig.5). While the effects of pumping on EC are rather
372 small, TP, NH₄ and turbidity are all affected by pumping. The effects of pumping appear to be different for events in different
373 seasons; turbidity for example increases during pumping in July and December but decreases in May. The increase during the
374 December pumping is especially marked (R^2 Pumping intensity versus Turbidity = 0.77 , Table S13). TP decreases during
375 pumping in July ($R^2 = -0.67$) and October and increases in May ($R^2 = 0.6$). Event 2 seems to have started a major drop in
376 turbidity (more than 1000 FNU) that continued some time after pumping.

377



378

379 **Figure 4** Selected events showing dilution and peaks of water quality parameters, with hourly precipitation (mm/h)
 380 and hourly pumping activity (m³/h). Note that between events different scales of TP and turbidity were used to reveal
 381 the dynamics
 382



383

384 **Figure 5** Pumping and pumping effect patterns on water quality, blue blocks represent the pumping duration

385 **4. Discussion**

386 This study aimed at understanding the dynamics of N and P fluxes from the low-lying urban polder of Geuzenveld to
 387 downstream surface waters in order to eventually support water managers to mitigate eutrophication. Based on our high-
 388 resolution water quality measurements, we found that the surface-water chemistry at the polder outlet pumping station is
 389 governed by a complex combination of hydrological mixing and biogeochemical processing. In the following discussion, we
 390 start with the relatively straightforward dilution behavior of EC, followed by adding the impact of primary production (i.e.

391 algae growth) for understanding the NH_4 concentration patterns, and benthic primary producer and iron chemistry for
392 understanding the turbidity and TP concentration patterns.

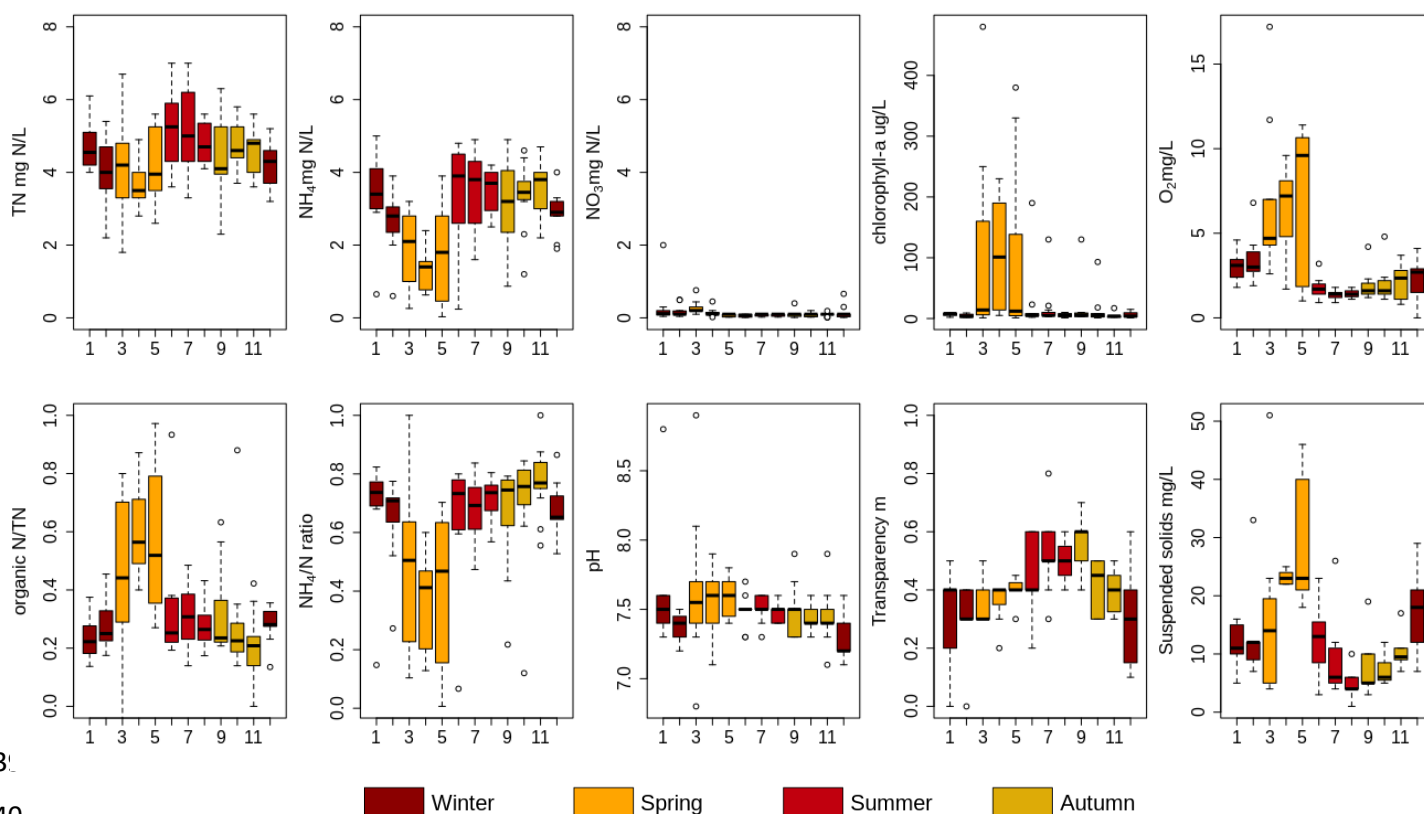
393 **4.1 Hydrological mixing between groundwater and rainfall**

394 In a highly manipulated low-lying urban catchment like Geuzenveld, mixing between rainwater and groundwater in the ditches
395 is fast due to the high fraction of impervious area and the installation of both a rainwater and a groundwater drainage system
396 that transport these contrasting water types efficiently to the ditches (Yu et al., 2019; Walsh et al., 2005). Runoff in Geuzenveld
397 has EC of about $166 \mu\text{S}/\text{cm}$ (Yu et al., 2019), which is lower than the groundwater EC ($1746 \mu\text{S}/\text{cm}$ on average). As a relatively
398 conservative water quality parameter (Figure S2), mixing between rainwater and groundwater should be the main process for
399 EC. This presumption is supported by the agreement between modelled and measured EC dynamics for the period between
400 May to November 2016. Precipitation events diluted the EC values at the pumping station, and the magnitude of dilution
401 depended on the intensity of precipitation; heavy rainfall resulted in low EC values (Fig.2D and Fig.4). In periods with absence
402 of rainfall, the EC values follow a recovery curve that resembles a linearly mixed reservoir with concentrations increasing to
403 values that approach the EC of the continuous groundwater supply of around $1500 \mu\text{S}/\text{cm}$. After November 2016, the
404 conservative mixing approach underestimated the EC but the main dynamics were still reproduced and the amplitude of the
405 EC dynamics remains similar to the model results, except for the short period Nov 20th- to Dec 1st 2016. Starting around Nov
406 20th, the EC started to increase relative to the dry season before. It coincides with an intensive pumping event after the first
407 intensive rainfall event that happened after a prolonged period of cumulative water deficit. This may be related with a first
408 flush from the drain system that starts to be activated more strongly, thus removing clogged material and lowering the overall
409 resistance of the drain system for shallow and deep groundwater inflow (van der Velde et al., 2010). It suggests that this
410 triggered the inflow of somewhat more mineralized groundwater relative to the period before, creating a shift in the EC towards
411 $\sim 250 \mu\text{S}/\text{cm}$ higher values that continued during the remainder of the monitoring campaign. It appeared that it raised the EC,
412 but did not change the amplitude or dynamics of the EC during the remainder of that period Fig 2 and 3, Table S6). An
413 alternative reason for the higher EC starting from November, 2016 on, would be the application of road salts during the winter
414 period. Although freezing conditions occurred from November onwards, we did not find any evidence for the prolonged effects
415 of road salts, as the chloride concentrations in the grab samples only showed two higher measurements, one in December 2016
416 and one in January 2017 (see Supplement, Figure S2.) So, overall, the observed dynamics of EC are consistent with mixing of
417 high EC seepage water with low EC runoff water.

418 During winter, mixing can also explain the dynamics of NH_4 and TP (Fig.3). Compared with groundwater, which carries
419 around $8 \text{ mg L}^{-1} \text{ NH}_4$ and $1.6 \text{ mg L}^{-1} \text{ TP}$, rain and runoff have much lower nutrient concentrations, which makes groundwater
420 the main nutrients source (Yu et al., 2019). Nutrients derived from groundwater mix with rainwater in the ditches through
421 direct seepage and the efficient groundwater drainage systems. Clearly, NH_4 is diluted during the rain events and a gradual
422 increase of NH_4 starts after each rain event during the wet season showing slopes that resemble the model reconstruction. Over
423 the whole period, measured NH_4 concentrations are overestimated by the model, indicating that some NH_4 is probably lost to
424 transformation processes. This is especially true in the spring season of 2017, where NH_4 concentrations must be controlled
425 by other processes. Concentrations of TP are generally far below the conservative model reconstruction, except between the
426 end of November and the beginning of March. During this particular period the minimum measured TP concentrations are
427 captured nicely by the conservative model, however distinct peaks up to 3 mg L^{-1} are not captured by the model and must have
428 different physical or chemical processes determining them. While the mixing process can explain part of the dynamics of NH_4
429 and TP in the wet season, the mixing assumption cannot explain the behavior of NH_4 and TP during other seasons, when NH_4
430 and TP measured time series drift far below from the conservative mixing model pattern because of biological and chemical
431 processes.

432 **4.2 Primary production and nutrients**

433 NH₄ dynamics during winter can be explained by mixing. However, biological processes are overruling the mixing process
 434 during spring and summer. It resulted in lower measured NH₄ concentrations than modeled during this period. Studies have
 435 shown that benthic and planktonic primary producers (e.g. phytoplankton) assimilate nutrients and are an important factor
 436 controlling nutrient dynamics in rivers, lakes, and streams (Hansson, 1988; Jäger et al., 2017). In polder Geuzenveld, the
 437 biological nutrient uptake is not only reflected in the time series data (Fig.2 and 3, Table S3) but is also evident in the monthly
 438 measurements from the water authority for the period 2007-2018, as summarized in Figure 6 and Table S15-S19.



439

440

441 **Figure 6 Monthly measurements of TN, NH₄-N, NO₃-N, chlorophyll-a, O₂ organic N/ TN and NH₄-N/TN (NH₄/N)**
 442 **mass ratio, pH, water transparency, and suspended solids in Geuzenveld from 2007 to 2018. X axis is month.**

443

444 The increasing availability of light (and temperature increase) during spring (Figure S6), induces growth of primary producers.
 445 Growth of primary producers results in consumption of ammonium, phosphate and a production of organic-N, chlorophyll-a,
 446 oxygen, and suspended solids, and led to a relatively higher pH because of the uptake of CO₂ (Figure 6, Table S16). These
 447 patterns are also clearly reflected in the shift in the NH₄/TN and organic-N/TN ratios during spring (Figure 6). Primary
 448 production occurs both in the water column by phytoplankton as well as by benthic algae. Macrophytes could in principle also
 449 contribute, but they were absent in Geuzenveld. One of the structuring factors governing the relative importance of benthic
 450 and planktonic primary producers is light availability: benthic algae and macrophytes tend to dominate in shallow and clear
 451 waters, while phytoplankton is more likely to dominate in deeper and more turbid waters (Hartwig, 1978; Jäger and Borchardt,
 452 2018; Petranich et al., 2018; Middelburg, 2019). Although our data do not allow conclusive determination whether benthic or
 453 pelagic primary producers dominate, it appears that their relative importance varies with season.

454 These primary producers also compete for nutrients. Benthic primary producers have direct (macrophytes) or first (benthic
 455 algae) access to nutrients that seep up from the subsurface, while planktonic primary producers depend on nutrient supply from
 456 surface runoff and nutrients remaining after consumption by benthic primary producers. For example, Henry and Fisher (2003)
 457 found that benthic algae can remove up to 80% of nitrogen from an upwelling water source. As we stated above, nutrient-rich

458 groundwater is the major source of N and P to surface waters in polder Geuzenveld. In addition, due to the shallow depth of
459 the ditches, light reaches the bottom with the consequence that benthic algae can proliferate in this polder. These benthic
460 primary producers might utilize the up-flowing nutrients from groundwater and intercept the nutrients from seeping further
461 into the water column (Hansson, 1988; Pasternak et al., 2009). The increasing light availability and thus primary production
462 during spring led to the nearly complete deprivation of NH_4 in the water column (Fig.2C).

463 Following the spring bloom, concentrations of chlorophyll-a (proxy for phytoplankton biomass) and O_2 dropped substantially,
464 while NH_4 concentrations rapidly recovered to around 4 mg L^{-1} in both the time series (Fig.2C) and the long-term monthly
465 sampling results (Fig.6). Dissolved O_2 remained low (close to hypoxia) during the whole summer (below 2 mg L^{-1}) (Fig.2E
466 and Fig.6), indicating that oxygen consumption by organic matter degradation and re-oxidation of reduced components from
467 groundwater seepage outcompeted oxygen production from primary production. During summer, suspended solid and
468 chlorophyll-a concentrations were low (Fig.6), indicating low biomass of plankton algae. Suspended solid and phytoplankton
469 dominate light attenuation (Scheffer, 1998; Middelburg, 2019). Consequently, during this period, we observed an abrupt shift
470 of the water regime from a turbid state to completely clear, as reflected in the high transparency from June to September (Fig.
471 6). The low biomass of phytoplankton might be due to N limitation as nutrients are intercepted by benthic algae at the sediment
472 interface. An alternative explanation is that zooplankton grazing maintained phytoplankton biomass low (Strayer et al., 2008;
473 Genkai-Kato et al., 2012).

474 Temperature and light reaching the sediment started to fall from September onwards (Figure S6), thereby reducing the intensity
475 of biological activity, including NH_4 assimilation. Consequently, NH_4 started to behave conservatively again like EC (Fig.2 &
476 Fig.3). The best fit between the modeled and measured NH_4 was from the end of November to the beginning of March, i.e.
477 during the winter period with lower light levels and shorter day lengths and very low primary production. The absence of
478 primary production during winter, leads to conservative behavior of NH_4 governed by the mixing between groundwater and
479 rain water.

480

481 **4.3 P binding and turbidity**

482 Iron chemistry is considered the dominant process governing the P dynamics in shallow groundwater fed ditches (Lijklema,
483 1994; Smolders et al., 2006; van der Grift et al., 2018). However, primary producers take up P for growth and at the same time
484 release O_2 that regulates iron chemistry in lake water column (Table S1-S3, Spear et al., 2007; Zhang and Mei, 2015; Lu et al.,
485 2016). This web of interactions likely controls P dynamics in these ditches.

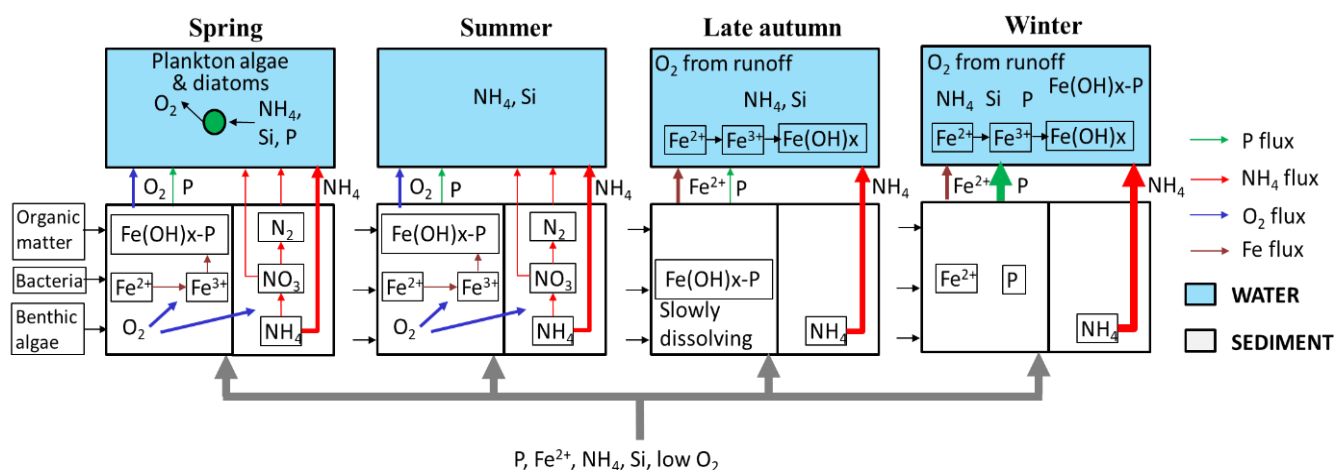
486 From spring to autumn, TP concentrations were fluctuating around 0.5 mg L^{-1} , and the water had low turbidity ($<50 \text{ FNU}$),
487 thus high transparency allowing the growth of benthic algae that produce oxygen. Consequently, when P and Fe rich anoxic
488 groundwater reaches the surface water-sediment interface, Fe oxidized into iron hydroxides in a short time (Van der Grift et
489 al., 2014). P is then sorbed onto those Fe-hydroxides and retained in the sediments. Oxidation of reduced iron consumes O_2 ,
490 contributing to the low O_2 conditions of the water column (Fig.2E). Moreover, it leads to the formation of a reddish-brown
491 film of ferric iron (hydrated ferric oxide, Baken et al., 2013; van der Grift et al., 2018) on the bottom of the ditches, which can
492 be seen in summer when the water was transparent. This slimy layer comprising iron hydroxides and benthic microbes can
493 easily be resuspended and therefore act as a source of turbidity following perturbations by pumping, wind, rain or foraging
494 fish, e.g. event 1 (Fig.5). Lu et al (2016) showed that co-precipitation of P with metal oxides was stimulated by periphytic
495 biofilm activity that increased the water pH. Consistently, a relatively higher pH was also observed in our spring monthly
496 samples (Fig.6).

497 From the late autumn onwards, turbidity and total Fe concentrations substantially increased compared to the rest of the time
498 (Fig.2, p value < 0.001 for turbidity and $= 0.02$ for Fe). Turbidity peaked first at 1800 FNU and stayed at a plateau of ~ 200
499 NFU during the rest of the cold and wet season. Total Fe in the water column reached to 6 mg L^{-1} from below 1 mg L^{-1} . During
500 this period the water turned brownish and transparency declined (Fig.6). Iron-rich particles are the most likely source of

501 turbidity in freshwater (Lyvén et al., 2003; Gunnars et al., 2002; and Lofts et al., 2008). The suspension of these brownish iron
 502 colloids was likely stabilised by the presence of the dissolved organic matter (Mosley et al., 2003; Van der Grift et al., 2014),
 503 which (DOC) increased up to 18~33 mg L⁻¹ during events (Supplementary information Figure S4). In the late autumn, the
 504 anoxic/oxic interface shifts from the sediment into the water column and so does the locus of colloid formation. The ditch
 505 sediment, which had benthic algae activity releasing O₂ during spring and summer, became anoxic in the fall by the upwelling
 506 of the anoxic groundwater. The anoxic seepage occurs year-round, but the production of oxygen by the benthic algae creates
 507 an anoxic-oxic transition at the water-sediment interface, which leads to iron hydroxides precipitation in the slimy layer at the
 508 bottom that disappears after the algae die off. As a consequence, Fe oxidation moved into the water column where the
 509 conditions were relatively oxic (Van der Grift et al., 2014). Nevertheless, there was probably still enough Fe or other mineral
 510 oxides, such as aluminum hydroxide (Kopáček et al., 2005), binding capacity in the sediment for the fixation of P, as P
 511 concentrations remained low during this first turbidity peak. We suggest that the turbidity peak of 1800 FNU is caused by the
 512 mineralisation of the benthic algae once they die off when light and temperature conditions decrease, combined with the shift
 513 of ironhydroxide formation from the sediment-water interface to the water column. The latter process continues through the
 514 whole winter season, until primary production restarts in spring (Figure 7).
 515 During winter, temperatures were below 5°C, pH values were relatively lowered, and TP achieved its peak concentrations
 516 (Fig.2D). During this period, iron reduction in the sediments continued, P bounded to iron oxides gradually got released along
 517 with reduced iron (Li et al., 2016). In the water column, reduced iron was oxidized but much slower than during spring-autumn
 518 due to the lower temperatures (Van der Grift et al., 2014), and dissolved P was incorporated in iron flocs with the result that
 519 particulate P concentrations and turbidity became high (Table S1, R² for Fe~turbidity 0.81, TP~Fe 0.65; Table S2, Fe~turbidity:
 520 R² = 0.72, , TP grab~Fe 0.79; Yu et al., 2019).

521 4.4 Process synthesis

522 With the presence of benthic algae, abundant organic matter and bacteria, the sediment functions as an active environment for
 523 biotic processes (such as primary production and nitrification-denitrification-anammox) and abiotic processes (such as iron
 524 oxidation). Figure 7 shows a conceptual diagram for the N and P dynamics in this lowland urban catchment during the four
 525 seasons which summarizes our hypotheses about the functioning of the system.



526
 527 **Figure 7 Schematic representation of N and P dynamics in spring, summer, later autumn and winter. The thickness of the flow lines**
 528 **represents the concentration magnitudes, the thicker the line, the higher the concentrations.**
 529

530 **Spring:** The improved light (and temperature) conditions stimulated primary production and nutrient uptake (N, P, Si) by
 531 phytoplankton and benthic algae. The resulting oxygen production caused oxidation of reduced iron from groundwater and the
 532 formation of iron oxides at the sediment surface. P was mostly bounded to this particulate iron instead of being released into

533 the upper water layer. In this period turbidity was relatively low, but suspended solids reached a high concentration due to the
534 phytoplankton.

535 **Summer:** N and P were still being removed by biological processing, in particular by benthic algae. Phytoplankton biomass
536 decreased because of competition for N or grazing activity. Benthic algae produced O₂, which in turn was used to oxidize all
537 reduced iron reaching the sediment-water interface and P was still retained by iron hydroxides in the sediment. The water
538 column was transparent (low TP and phytoplankton biomass) and relatively low in oxygen due to the continuous supply of
539 anoxic groundwater, the mere absence of O₂-rich runoff, the oxidation process of Fe(II) and possibly by microbial organic
540 matter decomposition during warm periods with relatively stagnant water.

541 **Late autumn:** Biological activity declined (colder and less light), and more NH₄ reached the water column. Moreover, the
542 redox zone moved from the sediment-water interface into the water column (Van der Grift et al. 2014, 2016); the oxidation of
543 Fe in the water column caused a peak of turbidity. P was still sequestered to minerals in the sediment.

544 **Winter:** During winter, NH₄ and TP showed the highest concentrations because of low biological activity. Iron oxides in the
545 sediment dissolved under reductive and organic matter abundant conditions and released Fe²⁺ and P into the water column
546 increasing P concentrations therein. NH₄ and EC dynamics were primarily governed by the conservative mixing between
547 groundwater and precipitation/runoff.

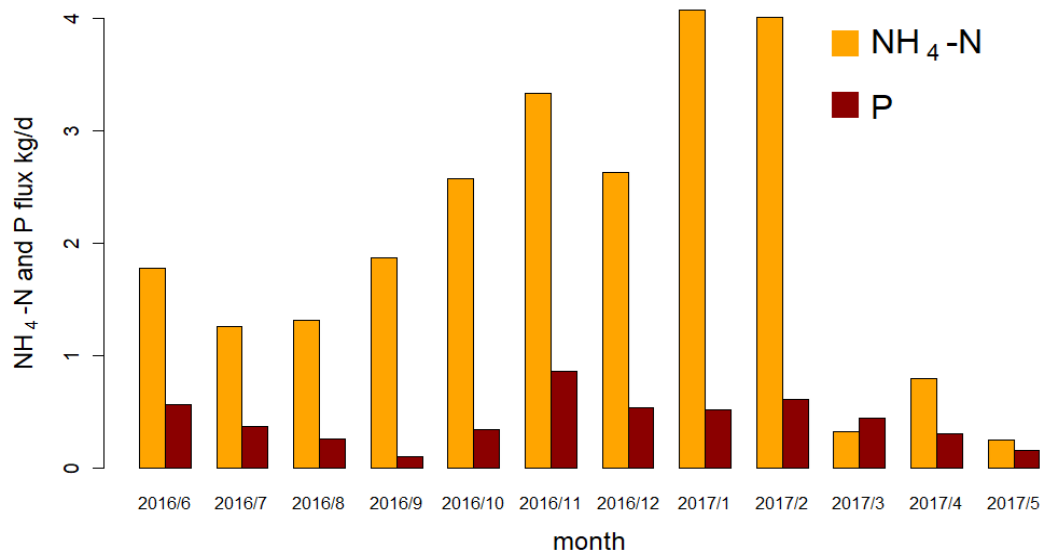
548 **4.5 Event scale N and P dynamics**

549 At the event scales, NH₄ and EC were reduced by dilution from precipitation/runoff. For P and turbidity there was no clear
550 relation to precipitation events, except for events in late autumn and winter (e.g. Figure 4, event 3). The responses to
551 precipitation and pumping events were different from those reported in the literature. Rozemeijer et al. (2010b) studied an
552 agricultural catchment and found that rainfall events led to NO₃ decreases and P increases. Miller et al. (2016) observed NO₃
553 decreases during large discharges in an urban catchment. The lowering of turbidity in our urban catchment during the dilution
554 periods that was associated with the winter events 3 and differs from observations in literature (van der Grift et al., 2014,
555 Rozemeijer et al., 2010b). In agriculture areas, turbidity usually peaks in response to rainfall events due to erosion and
556 remobilization of sediments. In an urban, paved environment erosion may be limited and runoff water has a low turbidity.
557 Moreover, in the case of turbid pre-event conditions, fresh precipitation water flushes away this turbid water. In addition, Yu
558 et al. (2019) showed that precipitation runoff delivers particles and O₂ to the ditches. We suggest that this accelerates the
559 further aggregation of the iron complexes; the resulting larger particles more readily settle to the bottom, causing a reduction
560 of turbidity during the events itself (Fig. 4, EC dilution part of events 3 and 4).

561 In artificial lowland catchments, water systems are intensively regulated by pumping activity to prevent flood and drought.
562 However, there is a substantial lack of knowledge about the possible consequences of such regulation on aquatic ecology and
563 water quality. Peaks in P and turbidity by the activation of pumps was observed by Van der Grift et al. in their high frequency
564 monitoring campaign in an agriculture lowland polder (Van der Grift et al., 2014 & 2016). This type of event scale dynamics
565 would be easily missed in a daily or lower frequency sampling schedule, especially because pumping occurs almost solely
566 overnight in our regulated catchments. As such, only a sampling schedule with 7 hours intervals (e.g. Neal et al. 2011) or high-
567 frequency monitoring is able to catch the short-term dynamics (Van Geer et al. 2016).

568 Contrary to the findings of Van der Grift et al. (2014, 2016), the effects of pumping activity on N, P and turbidity dynamics
569 were variable, depending on the season. During the phytoplankton bloom in spring, activation of pumps resulted in flushing
570 and as a result reduced turbidity during the event (Fig. 5 event 4). Consequently, phytoplankton was transferred to the
571 downstream channel and added to the total N pool in that system. In summer (Fig.5 event 1), the dead detritus and the layer of
572 iron compounds at the sediment surface were easily resuspended and contributed to turbidity peaks at the beginning of the
573 pumping, but the materials also re-sedimented almost immediately once the flow reached stability. Resuspension also resulted
574 in an increase of NH₄ in the water column which then was being pumped out (Fig.5 event 1). During late autumn, we observed

575 that the water was highly turbid (see also Yu et al. 2019) which we suggest to be caused by the formation of iron hydroxide
 576 colloids in the water column, which is supported by correlations between Fe-grab and Turbidity ($R^2= 0.72$, Table S2). We
 577 explain the reduced turbidity after a precipitation event as a result of the activation of the pumps which caused the export of
 578 the turbid water towards the receiving boezem in combination with aggregation of iron hydroxides in the water column and
 579 subsequent settling of the aggregates due to the supply of new O_2 -rich water (Fig.5 event 2, see also Van der Grift, et al., 2014).
 580 Moreover, NH_4 increased again by the pumping activity and was transferred downstream (Fig.5 event 2). The eventual impact
 581 of regulation of the Geuzenveld water system turns the pumping discharge into a point source for nutrients to downstream
 582 water bodies as shown in Figure 8.



583
 584 **Figure 8 Average daily NH_4 -N and P flux (kg per day) in each month in the discharge (calculated from the continuous**
 585 **measurements) of polder Geuzenveld from June 2016 to May 2017.**

587 Fluxes of N and P were highest during winter (Fig 6). These high fluxes are caused not only by the more frequent pumping
 588 activity, but also by the higher concentration of N and P in the water column in winter. In the time series data, NH_4 (the major
 589 form of N), had concentrations above 2.4 mg N L^{-1} (the local environmental quality standard (EQS) for N-total), in all seasons
 590 except spring. NH_4 concentrations even reached up to 6.5 mg L^{-1} . TP concentrations were constantly higher than 0.15 mg P L^{-1}
 591 (the local EQS); during winter it was always over 1 mg P L^{-1} . Although the NH_4 flux in the discharge was very low in spring
 592 (Fig.8), the actual total N flux might have been much higher, as organic N (phytoplankton) was the major form of TN instead
 593 of NH_4 during this period (Fig.6 NH_4 /N and organic-N/TN). Therefore, even though water authority measures have been
 594 effective in controlling the water quantities in the polder, it had unanticipated impact on nutrients export to the downstream
 595 water bodies. In order to prevent eutrophication in the urban waters, nutrient rich discharge from these areas is exported directly
 596 to the North-Sea Canal and to the North Sea.

598 4.6 Implications for urban water management in low lying catchments

599 This study demonstrated high frequency monitoring technology to be an effective tool for understanding the complex water
 600 quality dynamics. Investment in high frequency monitoring would greatly benefit the management of urban lowlands with
 601 substantial groundwater seepage by elucidating the principle biogeochemical processes and nutrient temporal patterns for
 602 realizing efficient mitigation and control of eutrophication. For example, redirecting the drain water effluent into constructed
 603 wetlands could be considered as a mitigation measure in low lying areas with artificial water systems that resemble the
 604 Amsterdam region, e.g. in cities such as New Orleans, Shanghai and Dhaka. Centralizing the treatment of discharge water is

605 also recommended, for instance by harvesting N as phytoplankton from the discharge during spring, or filtrating P at the
606 pumping station during winter. Measures that artificially increase oxygen concentrations in the waters, such as the inlet of
607 oxygen rich water, aeration by fountains or the artificial introduction of grazers or macrophytes may be considered to improve
608 the ecological status of these urban waters. Moreover, aeration of the water in summer and autumn would possibly enhance
609 processes such as coupled-nitrification-denitrification and anammox, eventually converting NH_4 to N_2 , before the water is
610 discharged to downstream waters. Importantly, before the application of any measures or maintenance in urban low-lying
611 catchments, managers should evaluate the potential effects on the biological and chemical resilience, e.g. dredging of a layer
612 with abundant benthic activity might destroy an important buffer to nutrients in growing seasons, especially P.

613 In this study, we focused on the analysis of the temporal patterns of water composition and on the deduction of the potential
614 biogeochemical processes. Detailed studies about these processes and the biotic communities at the sediment-water interface
615 were outside of the scope of this paper. A comprehensive study on the sediment-water interface would be necessary to further
616 increase our knowledge on the role of the benthic zone in attenuating N and P seeping up from groundwater. Besides, further
617 research would need to consider the optimal physical dimensions of water courses and drain configurations, as to benefit the
618 ecological status of urban waters that are prone to nutrient-rich groundwater seepage.

619

620 5. Conclusions

621 This study aimed at improving our understanding of the mechanisms that control the temporal patterns of nutrients and other
622 water quality parameters in an urban catchment. Time series of EC, NH_4 , TP, and turbidity were obtained by applying a high
623 frequency monitoring technology for one year (May 2016 to July 2016). Observed EC, NH_4 and TP could only partly be
624 explained by conservative mixing of groundwater and precipitation components. In particular, N and P fluxes in the shallow
625 ditches were also impacted by biogeochemical processes, such as primary production and iron redox transformations.

626 (1) NH_4 , the dominant form of N in surface water, originates primarily from groundwater seepage, and concentrations
627 are lowered by primary producers (phytoplankton and benthic algae) in the growing season. High algal biomass was
628 also clear from high chlorophyll-a and suspended solids in the water column.

629 (2) TP showed high concentrations in winter, but relatively low concentrations in other seasons. Iron redox chemistry
630 was the principle process controlling the P dynamics in shallow groundwater fed ditches. P dynamics may also have
631 been partly influenced by primary production which consumes P for growth and at the same time produces O_2
632 influencing the redox status in the sediments and in the water column.

633 (3) High turbidity levels occurred in the late autumn and winter, mostly in the form of iron hydroxides. It resulted from
634 a shift of the anoxic/oxic interface where the formation of iron hydroxides moves from the sediment towards the
635 water column.

636 (4) Water pumped from the polder to downstream water bodies was rich in NH_4 from summer to winter, but rich in
637 organic N in the form of algae during spring. P leaves the polder mainly during the winter season when it is released
638 from the sediment and exported mostly in the form of P sorbed to $\text{Fe}(\text{OH})_3$ colloids and as dissolved P.

639 (5) Precipitation diluted concentrations of most water quality parameters, but delivered O_2 to the water column, and in
640 that way indirectly affected P and turbidity by intensifying iron oxidation and precipitation.

641 (6) Unlike many other natural and artificial catchments, rainfall and pumping events did not increase turbidity or TP
642 concentrations at the short time scale, rather reduced turbidity and TP because of enhanced iron hydroxide
643 precipitation due to oxygen inputs by runoff.

644 Our understanding of the N and P dynamics in this low-lying urban catchment may contribute to the development of effective
645 water management strategies that reduce eutrophication conditions in both the urban polders and the downstream waters.
646 Drainage of very low-lying areas (for use as residential and/or agricultural areas) not only increases pumping costs, but can

647 also result in difficult to manage water quality conditions. Controlling the source, redirecting and utilizing the drainage water
648 might be strategies to reduce the input of N and P from groundwater into surface water. In addition, we showed that in lowland
649 urban areas with high seepage rates the reactivity of the stream bed sediments largely controls water quality of surface waters
650 and thus should be managed with care when cleaning the surface water systems.

651 **Acknowledgements**

652 This work was funded through China scholarship council (no. 201309110088) and supported by Waternet, the Strategic
653 Research Funding of TNO and Deltares. We highly appreciate the help and support from our Waternet co-workers: Eelco
654 Wiebenga, Henk Molenaar, Sonja Viester, Laura Moria, and Frank Smits.

655 **Code/data availability:** The code scripts and datasets related to this paper are available on request to Liang Yu, contact is
656 xiaobaidrawing@gmail.com.

657

658 **Author contribution:** Maarten Ouboter, Joachim Rozemeijer, and Hans Peter Broers funded this research. Hans Peter Broers
659 and Joachim Rozemeijer designed the field work. Liang Yu carried out the field work and the data collection, analysis,
660 visualization, discussion, and the writing of the manuscript, under the supervision of Hans Peter Broers and Joachim
661 Rozemeijer before 2019, Ype van der Velde as the main supervisor since 2019. All the authors participated the discussion of
662 the data analysis results, and helped prepare the manuscript.

663

664 **Competing interests:** The authors declare that there is no conflict of interest.

665 **References**

666 Audet J., Zak D., Bidstrup J., and Hoffmann C.C.. Nitrogen and phosphorus retention in Danish restored wetlands. Royal
667 Swedish Academy of Sciences, 1-13, 2019.

668 Bunch N.D. and Bermot M.J.. Nitrate and ammonium uptake by natural stream sediment microbial communities in response
669 to nutrient enrichment. *Research in Microbiology*, 163(2): 137-141, 2012.

670 Beusen A.H.W., Bouwman A.F., van Beek L.P.H., Mogollón J.M., and Middelburg J.J.. Global riverine N and P transport to
671 ocean increased during the 20th century despite increased retention along the aquatic continuum. *Biogeosciences*. 13: 2441-
672 2451, 2016.

673 Bierzoza M.Z., Heathwaite A.L., Bechmann M., Kyllmar K., and Jordan P.. The concentration-discharge slope as a tool for
674 water quality management. *Science of the Total Environment*, 630: 738-749, 2018.

675 Baken S., Sjostedt C., Gustafsson J.P., Seuntjens P., and Desmet N.. Characterisation of hydrous ferric oxides derived from
676 iron-rich groundwaters and their contribution to use suspended sediment of streams. *Applied Geochemistry*, 39: 59-68, 2013.

677 Cavaliere E. and Baulch H.M.. Winter nitrification in ice-covered lakes. *PLoS ONE*, 14(11): e0224864, 2019.

678 Chen M., Ding S., Chen X., Sun Q., Fan X., Lin J., Ren M., Yang L., and Zhang C.. Mechanisms driving phosphorus release
679 during algal blooms based on hourly changes in iron and phosphorus concentrations in sediments. *Water Research*, 133: 153-
680 164, 2018.

681 Díaz P., Stanek P., Frantzeskaki N., and Yeh D.H.. Shifting paradigms, changing waters: Transitioning to integrated urban
682 water management in the coastal city of Dunedin, USA. *Sustainable Cities and Society*. 26: 555-567, 2016.

683 Duncan J.M., Welty C., Kemper J.T., Groffman P.M., and Band L.E.. Dynamics of nitrate concentration-discharge patterns in
684 an urban watershed. *Water Resources Research*, 53: 7349-7365, 2017.

685 Eggimann S., Mutzner L., Wani O., Schneider M.Y., Spuhler D., de Vitry M.M., Beutler P., and Maurer M.. The Potential of
686 Knowing More: A Review of Data-Driven Urban Water Management. *Environmental Science & Technology*, 51: 2538-2553,
687 2017.

688 Filippelli M.G.. The global phosphorus cycle: Past, present, and future. *Elements*, 4(2): 89-95.

689 Fletcher T.D., Shuster W., Hunt W.F., Ashley R., Butler D., Arther S., Trowsdale S., Barraud S., Semadeni-Davies A.,
690 Bertrand-Krajewski J.L., Mikkelsen P.S., Rivard G., Uhl M., Dagenais D., and Viklander M.. SUDS, LID, BMPs, WSUD
691 and more – The evolution and application of terminology surrounding urban drainage. *Urban Water Journal*, 12(7): 525-542,
692 2015.

693 Griffioen J.. Extent of immobilisation of phosphate during aeration of nutrient-rich, anoxic groundwater. *Journal of Hydrology*,
694 320 (3-4): 359-369, 2006.

695 Gunnars A., Blomqvist S., Johansson P., and Andersson C.. Formation of Fe (III) oxyhydroxide colloids in freshwater and
696 brackish seawater, with incorporation of phosphate and calcium. *Geochim. Cosmochim. Acta*, 66 :745-758, 2002.

697 Genkai-Kato M., Vadeboncoeur, Liboriussen L., and Jeppesen E.. Benthic-planktonic coupling, regime shifts, and whole-lake
698 primary production in shallow lakes. *Ecology*, 93(3): 619-631, 2012.

699 Hartwig E.O.. Factors affecting respiration and photosynthesis by the benthic community of a subtidal siliceous sediment.
700 *Marine Biology*, 46: 283-293, 1978.

701 Hansson L.A.. Effects of competitive interactions on the biomass development of planktonic and periphytic algae in lakes.
702 *Limnology and Oceanography*, 33(1): 121-128, 1988. Henry J.C. and Fisher S.G.. Spatial segregation of periphyton
703 communities in a desert stream: causes and consequences for N cycling. *Journal of The North American Benthological Society*,
704 22 (4): 511-527, 2003.

705 He S. and Xu Y.J.. Three decadal inputs of nitrogen and phosphorus from four major coastal rivers to the summer hypoxic
706 zone of the northern Gulf of Mexico. *Water, Air, and Soil Pollution*, 226: 311, 2015.

707 Jäger C.G. and Borchardt D.. Longitudinal patterns and response lengths of algae in riverine ecosystems: A model analysis
708 emphasizing benthic-pelagic interactions. *Journal of Theoretical Biology*, 442: 66-78, 2018.

709 Jäger C.G., Hagemann J., and Borchardt D.. Can nutrient pathways and biotic interactions control eutrophication in riverine
710 ecosystems? Evidence from a model driven mesocosm experiment. *Water Research*, 115: 162-171, 2017.

711 Kuenen J.. Anammox bacteria: from discovery to application. *Nature Reviews Microbiology*, 6: 320-326, 2008.

712 Kopáček J., Borovec J., Hejzlar J., Ulrich K., Norton S.A., and Amirbahman A.. Aluminum control of phosphorus sorption by
713 lake sediments. *Environmental Science & Technology*, 39 (22): 8784-8789, 2005.

714 Kleeberg A., Hupfer M., and Gust G.. Phosphorus entrainment due to resuspension in a lowland river, Spree, NE Germany-A
715 laboratory microcosm study. *Water, Air, and Soil Pollution*, 183(1-4): 129-142, 2007.

716 Kabenge M., Wang H., and Li F.. Urban eutrophication and its spurring conditions in the Murchison Bay of Lake Victoria.
717 *Environmental Science and Pollution Research*, 23: 234-241, 2016.

718 Lijklema L.. Nutrient dynamics in shallow lakes: effects of changes in loading and role of sediment-water interactions.
719 *Hydrobiologia*, 275/276: 335-348, 1994.

720 Le Moal M., Cascuel-Oudou C., Menesguen A., Souchon Y., Etrillard C., Levain A., Moatar F., Pannard A., Souchu P.,
721 Lefebvre A., and Pinay G.. Eutrophication: A new wine in an old bottle. *Science of the Total Environment*, 651: 1-11, 2019.

722 Lyvén B., Hassellöv M., Turner D.R., Haraldsson C., and Andersson K.. Competition between iron- and carbon-based colloidal
723 carries for trace metals in a freshwater assessed using flow field-flow fractionation coupled to ICPMS. *Geochimica et*
724 *Cosmochimica Acta*, 67(20): 3791-3802, 2003.

725 Li H., Song C.L., Cao X.Y., and Zhou Y.Y.. The phosphorus release pathways and their mechanisms driven by organic carbon
726 and nitrogen in sediments of eutrophic shallow lakes. *Science of the Total Environment*, 572: 280-288, 2016.

727 Lofts S., Tipping E., and Hamilton-Taylor J.. The Chemical Speciation of Fe(III) in Freshwaters. *Aquatic Geochemistry*, 14(4):
728 337-358, 2008.

729 Lu H., Wang J., Li J., Shao H., and Wu Y.. Periphytic biofilm: A buffer for phosphorus precipitation and release between
730 sediments and water. *Chemosphere*, 144: 2058-2064, 2016.

731 Middelburg J.J.. *Marine Carbon Biogeochemistry - A Primer for Earth System Scientists*. Springer Briefs in Earth System
732 Sciences. Switzerland, 2019.

733 McGlathery K.J., Anderson I.C., and Tyler A.C.. Magnitude and variability of benthic and pelagic metabolism in a temperate
734 coastal lagoon. *Marine Ecology Progress Series*, 216: 1-15, 2001.

735 Mosley L.M., Hunter K.A., and Ducker W.A.. Forces between Colloid Particles in Natural Waters. *Environmental Science &*
736 *Technology*, 37 (15): 3303-3308, 2003

- 737 Middleburg J.J. and Nieuwenhuize J.. Uptake of dissolved inorganic nitrogen in turbid, tidal estuaries. *Marine Ecology*
738 *Progress Series*, 192: 79-88, 2000.
- 739 Miller M.P., Tesoriero A.J., Capel P.D., Pellerin B.A., Hyer K.E., and Burns D.A.. Quantifying watershed-scale groundwater
740 loading and instream fate of nitrate using high-frequency water quality data. *Water Resources Research*, 52: 330-347, 2016.
- 741 Mulder A., van de Graaf A.A., Robertson L.A., and Kuenen J.G.. Anaerobic ammonium oxidation discovered in a denitrifying
742 fluidized bed reactor. *FEMS Microbiology Ecology*, 1(16): 177-184, 1995.
- 743 Nyenje P.M., Foppen J.W., Uhlenbrook S., Kulabako R., and Muwanga A.. Eutrophication and nutrient release in urban areas
744 of sub-Saharan Africa-A review. *Science of the Total Environment*, 408: 447-455, 2010.
- 745 Neal, C., Reynolds, B., Norris, D., Kirchner, J. W., Neal, M., Rowland, P., Wickham H., Harman S., Armstrong L., Sleep D.,
746 Lawlor, A., Woods C., Williams B., Fry M., Newton G., Wright D.. Three decades of water quality measurements from the
747 Upper Severn experimental catchments at Plynlimon, Wales: an openly accessible data resource for research, modelling,
748 environmental management and education. *Hydrological Processes*, 25(24), 3818-3830, 2011.
- 749 Nizzoli D., Welsh D.T., and Viaroli P.. Denitrification and benthic metabolism in lowland pit lakes: The role of trophic
750 conditions. *Science of the Total Environment*, 703: 134804, 2020.
- 751 Painter H.A.. A review of literature on inorganic nitrogen metabolism in microorganisms. *Water Research*, 4: 393-450, 1970.
- 752 Pasterank A., Hillebrand H., and Flöder S.. Competition between benthic and pelagic microalgae for phosphorus and light-
753 long-term experiments using artificial substrates. *Aquatic Sciences*, 71: 238-249, 2009.
- 754 Putt A.E., MacIsaac E.A., Herunter H.E., Cooper A.B., and Selbie D.T.. Eutrophication forcings on a peri-urban lake
755 ecosystem: Context for integrated watershed to airshed management. *PLoS ONE*, 4(7): e0219241, 2019.
- 756 Paerl H.W., Scott J.T., McCarthy M.J., Newell S.E., Gardner W.S., Havens K.E., Hoffman D.K., Wilhelm S.W., and
757 Wurtsbaugh W.A. It Takes Two to Tango: When and Where Dual Nutrient (N & P) Reductions Are Needed to Protect Lakes
758 and Downstream Ecosystems. *Environmental Science & Technology*, 50: 10805-10813, 2016.
- 759 Rozemeijer J.C. and Broers H.P.. The groundwater contribution to surface water contamination in a region with intensive
760 agricultural land use (Noord-Brabant, The Netherlands). *Environmental Pollution*. 148(3): 695-706, 2007.
- 761 Rozemeijer J.C., van der Velde Y., van Geer F.C., Bierkens M.F.P., and Broers H.P.. Direct measurements of the tile drain
762 and groundwater flow route contributions to surface water contamination: From field-scale concentration patterns in
763 groundwater to catchment-scale surface water quality. *Environmental Pollution*, 158: 3571-3579, 2010a.
- 764 Rozemeijer J.C., van der Velde Y., van Geer F.C., de Rooij G.H., Torfs P.J.J.F. and Broers H.P.. Improving load estimates for
765 NO₃ and P in surface water by characterizing the concentration response to rainfall events. *Environmental Science &*
766 *Technology*, 44 (16): 6305-6312, 2010b.
- 767 Rode M., Wade A.J., Cohen M.J., Hensley R.T., Michael J.B., Kirchner J.W., Arhonditsis G.B., Jordan P., Kronvang B.,
768 Halliday S.J., Skeffington R., Rozemeijer J., Aubert A.H., Rinke K., and Jomaa S.. Sensors in the stream: the high-frequency
769 wave of the present. *Environmental Science & Technology*, 50: 10297-10307, 2016.
- 770 Scheffer, M.. *Ecology of shallow lakes*, 1st edition. London: Chapman & Hall, 1998.
- 771 Spears B.M., Carvalho L., Perkins R., Kirika A., and Paterson D.M.. Sediment phosphorus cycling in a large shallow lake:
772 spatio-temporal variation in phosphorus pools and release. *Hydrobiologia*, 584: 37-48, 2007.
- 773 Smolders A.J.P., Lamers L.P.M., Lucassen E.C.H.E.T., Van Der Velde G., and Roelofs J.G.M.. Internal eutrophication: How
774 it works and what to do about it—a review. *Chemistry and Ecology*, 22(2): 93-111, 2006.
- 775 Strayer D.L., Pace M.L., Caraco N.F., Cole J.J., and Findlay S.E.G.. Hydrology and grazing jointly control a large-river food
776 web. *Ecology*, 89(1): 12-18, 2008.
- 777 Thamdrup B. and Dalsgaard T.. Production of N₂ through anaerobic ammonium oxidation coupled to nitrate reduction in
778 marine sediments. *Applied and Environmental Microbiology*, 68(3): 1312-1318, 2002.
- 779 Toor G.S., Occhipinti M.L., Yang Y.Y., Majcherek T., Haver D., and Oki L.. Managing urban runoff in residential
780 neighbourhoods: Nitrogen and phosphorus in lawn irrigation driven runoff. *PLoS ONE*, 12(6): e0179151, 2017.
- 781 Van der Grift, B., Broers, H.P., Berendrecht, W., Rozemeijer, J., Osté, L., and Griffioen, J.. High-frequency monitoring reveals
782 nutrient sources and transport processes in an agriculture-dominated lowland water system. *Hydrology and Earth System*
783 *Sciences*, 20(5): 1851-1868, 2016.

784 Van Geer F.C., Kronvang B., and Broers H.P.. High-resolution monitoring of nutrients in groundwater and surface waters:
785 process understanding, quantification of loads and concentrations, and management applications. *Hydrology and Earth System*
786 *Sciences*, 20: 3619-3629, 2016.

787 Van der Grift B., Osté L., Schot P., Kratz A., van Popta E., Wassen M., and Griffioen J.. Forms of phosphorus in suspended
788 particulate matter in agriculture-dominated lowland catchments: Iron as phosphorus carrier. *Science of The Total Environment*,
789 631-632: 115-129, 2018.

790 Van der Velde Y., Rozemeijer J.C., de Rooij G.H., van Geer F.C., Broers H.P.. Field-scale measurements for separation of
791 catchment discharge into flow route contribution. *Vadose Zone Journal*, 9(1): 25-35, 2010.

792 Van der Grift B., Rozemeijer J.C., Griffioen J., and van der Velde Y.. Iron oxidation kinetics and phosphate immobilization
793 along the flow-path from groundwater into surface water. *Hydrology and Earth System Sciences*, 18: 4687-4702, 2014.

794 Wilczak A., Jacangelo, J.G., Marcinko J.P., Odell L.H., and Kirmeyer G.J.. Occurrence of nitrification in chloraminated
795 distribution systems. *Journal AWWA*, 88(7): 74-85, 1996.

796 Wang T., Liu G., Gao L., Zhu L., Fu Q., and Li D.. Biological and Nutrient Responses to a Typhoon in the Yangtze Estuary
797 and the Adjacent Sea. *Journal of Coastal Research*, 32(2): 323-332, 2016.

798 Walsh C.J., Roy J.W., Feminella J.W., Cottingham P.D., Groffman P.M., and Morgan II R.P.. The urban stream syndrome:
799 current knowledge and the search for a cure. *Journal of The North American Benthological Society*, 24(3): 706-732, 2005.

800 Wriedt, G., Spindler J., Neef T., Meißner R., and Rode M.. Groundwater dynamics and channel activity as major controls of
801 in-stream nitrate concentrations in a lowland catchment system? *Journal of Hydrology*, 343: 154–168, 2007.

802 Yu L., Rozemeijer J.C., van Breukelen B.M., Ouboter M., van der Vlugt C., and Broers H.P.. Groundwater impacts on surface
803 water quality and nutrient loads in lowland polder catchments: monitoring the greater Amsterdam area. *Hydrology and Earth*
804 *System Sciences*, 22:487-508, 2018.

805 Yu L., Rozemeijer J.C., van der Velde Y., van Breukelen B.M., Ouboter M., and Broers H.P.. Urban hydrogeology: Transport
806 routes and mixing of water and solutes in a groundwater influenced urban lowland catchment. *Science of the Total*
807 *Environment*, 678: 288-300, 2019.

808 Yang Y.Y. and Toor G.S.. Stormwater runoff driven phosphorus transport in an urban residential catchment: Implications for
809 protecting water quality in urban watersheds. *Scientific Reports*, 8: 11681, 2018. doi: 10.1038/s41598-018-29857-x

810 Zhu W.X., Dillard N.D., and Grimm N.B.. Urban nitrogen biogeochemistry: status and processes in green retention basins.
811 *Biogeochemistry*, 71: 177-196, 2004.

812 Zhang W., Jin X., Meng X., Tang W., and Shan B.. Phosphorus transformations at the sediment-water interface in shallow
813 freshwater ecosystems caused by decomposition of plant debris. *Chemosphere*, 201: 328-334, 2018.

814 Zhang X. and Mei X.. Effects of benthic algae on release of soluble reactive phosphorus from sediments: a radioisotope tracing
815 study. *Water Science and Engineering*, 8(2): 127-131, 2015.

816 Zhou L., Wang S., Zou Y., Xia C., and Zhu G.. Species, abundance and function of ammonia-oxidizing Archaea in inland
817 waters across China. *Scientific Reports*, 5: 15969, 2015.